UNIVERSITÀ DEGLI STUDI DELL'AQUILA

DIPARTIMENTO DI MEDICINA CLINICA, SANITÀ PUBBLICA, SCIENZA DELLA VITA E DELL'AMBIENTE

Dottorato di Ricerca in medicina clinica e sanità pubblica
Curriculum Scienze Cardiovascolari

XXXIV ciclo

New pathogenetic mechanisms from impaired cell adhesion in cardiovascular diseases and genodermatoses

SSD: MED11

Dottorando

Rosanna Monetta

Matr.262364

Coordinatore del corso

Prof. Claudio Ferri

Tutor

Prof. Silvio Romano

Co-tutor

Prof. Francesco Brancati

a.a. 2020/2021

Index

Abstract

Difficulties in studying genetic disorders come from phenomena of pleiotropism and genetic heterogeneity which often produce phenotypic overlapping. The advent of next generation sequencing (NGS) and a multidisciplinary approach, based on the interplay of clinic, genetic and functional biology studies, give us the possibility to deep investigate and amplify/rewrite many genetic conditions. An example of this synergic approach is illustrated in this work thesis whose findings are: i) the identification of genetics variants known to be associated with Multiple Self-Healing Squamous Epithelioma which we found to be involved also in the onset of Loeys-Dietz syndrome, ii) expansion of the phenotypic spectrum of Bartsocas-Papas and Curly hair-ankyloblepharon-nail dysplasia syndromes associated with mutations in Receptor Interacting Serine/Threonine Kinase 4 (RIPK4), and identification of nectin-4 as a new player of the p63 molecular network modulated by RIPK4, iii) the identification of phenotypic variability resulting from different mutations in Connexin 26 (GJB2) resulting in non-syndromic or syndromic hearing loss. In conclusion, the studies presented in this thesis highlight the paramount importance for a correct clinical and molecular diagnosis to plan a personalized medical approach based on individual genetic makeup.

Introduction

Nosology is a branch of medical science that deals with the classification of diseases. An accurate nosology is essential for prognosis, appropriate follow-up, therapy and is used extensively in public health, to allow epidemiological studies of public health issues. In an earlier period, the physicians named genetic diseases using their own names, patient's names (i.e initials), or geographic designations. It is easy to guess that different methods to classify the same disease led to a big confusion among the physicians worldwide. Modern classification systems encourage an etiological approach, by including the disease-causative gene/molecule or pathway, if known, in the condition name. For example, a growing number of neurodevelopmental disorders (including so-called autism) has been recognized as a result of single gene mutations (e.g. RERE-Related Disorders). Also in the field of cardiovascular genetics, several cardiomyopathies are being linked to specific gene mutations and the different underlying genetic defect changes dramatically the prognosis and the therapeutical approach, as in the case of LMNA- or DSP-cardiomyopathy. In addition, over the last years, the identification of the pathogenic mechanism of a growing number of genetic disorders led the grouping of conditions under pathologically distinct "umbrellas" when convergent molecular mechanisms were identified (e.g. cohesinopathies; meaning disorders caused by genes encoding distinct cohesins or, similarly, rasopathies, etc.).

Another important topic in recognizing genetic disorders is the phenomena of pleiotropism and genetic heterogeneity. Pleiotropism means "many from one": multiple phenotypic features from one etiologic entity - one gene.[1] It means that mutations in one gene affect two or more traits; this is because a gene codes for a protein which serves multiple purposes in the cell, and catalyzes numerous reactions, interacting with various signal receptors or pathways. In this way, a single gene is able to have a remarkable impact on different systems. Actually, even mutations that do not directly alter any gene but are present in non-coding regions, such as changes in DNA copy number of protein-binding motifs or structural changes that alter chromatin architecture, can have a pleiotropic effect.[2]

Mutations in the *FBN1* gene encoding Fibrillin-1 represent an example of pleiotropic effect. Fibrillin-1 binds to other fibrillary proteins and other molecules to form threadlike filaments called microfibrils.[3] Microfibrils serve as "storage shelves" for the Transforming grow factor beta (TGFβ) ligand and release it in a regulated way.[3] TGFβ ligand binds the transforming grow factor receptor beta 1/2 (TGFBR1/2) on the cells' surface resulting in the phosphorylation of downstream cofactors (SMAD2/3) which induce the transcription of target genes. Therefore, mutations in the *FBN1* gene reduce the amount of functional protein, which leads to decreased microfibril formation, impairing

tissue integrity and elasticity and deregulating the release of TGFβ, with subsequent alterations of homeostasis and development of different tissues. Clinically, such mutations cause the Marfan syndrome, which is characterized by aortic root aneurysms, aortic dissection and mitral valve prolapse, joint hypermobility, limb elongation, scoliosis, iris transillumination defects and ectopia lentis .[3] Although at first glance the symptoms do not appear directly related to one another, we can find a common denominator in the presence of Fibrillin-1 as a fundamental component of connective tissue which, in turn, is a structural component of many elements such as bones, ligaments, muscles, blood vessels, heart valves, eyes and joints, explaining the pleiotropic effects deriving from mutations in this gene.

Genetic heterogeneity represents another critical concept for genotype-phenotype correlation and therefore for the classification of diseases. It means "one from many", that is a similar phenotype can be caused by several different etiologic factors, i.e. mutated genes[1]. The problem of a correct molecular diagnosis is given by the overlapping of phenotypes which makes it difficult to associate a specific feature with a single mutated gene. This is explainable because the products of different genes are assembled each other to form a single multimeric protein involved in a unique function, or are interconnected in a specific molecular pathway or different converging signaling pathways contributing to the homeostasis and development of a tissue or organ.

Several examples of genetic heterogeneity exist and will be illustrated in this thesis. For examples, ectodermal dysplasias (EDs) are a heterogenous group of hereditary disorders sharing structural and functional abnormalities in tissues derived from the ectoderm.[4] Most of these diseases are also combined with an abnormal development of structures derived from the mesenchyme. To date, approximately 200 conditions of such disorders are known, and pathogenic mutations have been identified in around 30 genes. Mutations in only 4 genes (*Ectodysplasin A*, *Ectodysplasin A* receptor, *EDAR associated death domain*, *WNT family member 10A*) are responsible for most of the cases of ED.[4] Biomolecular analyses identified two different pathogenic mechanisms through which these mutations act. The first mechanism corresponds to disorders in which the interaction between the ectoderm and the mesenchyme is impaired. The resulting clinical phenotype is hypoplasia or aplasia of structures derived from the ectoderm. Development and differentiation of these structures fail due to the absence of specific reciprocal signals between the ectoderm and the mesenchyme.[4] The second mechanism corresponds to disorders in which there is abnormal function of a structural protein in the cell membrane. Examples of structural proteins, including nectin1/4, connexins, plakophilin, whose roles in adhesion and cell-cell communication is essential for maintaining tissue homeostasis and controlling cell growth, development and response to different stimuli.[4] Clinically, these disorders

are mainly characterized by skin abnormalities such as palmoplantar keratoderma, with or without involvement of highly differentiated epithelia associated with deafness or retinal dystrophy.[4]

Hereditary connective tissue disorders (HCTD) are another example of conditions with overlapping features caused by alterations in genes encoding components that regulate the structure and function of the connective tissue.[5] These syndromes affect various organ systems such as skin, joints, bone, eyes, lungs, heart and blood vessels and often predispose patients to aortic pathology and in particular aortic dissection.[6] The discovery of these HCTD was followed by the identification of mutations in a wide range of genes encoding for structural proteins (e.g., *FBN1*, *COL1A1*, *COL3A1*, *COL5A1*, *BGN*), modifying enzymes (e.g., *ADAMTS2*, *PLOD1*), or components of the TGFβ-signaling pathways (e.g., *SMAD2/3*, *TGFBR1/2* and *TGFB2/3*).[7] Almost all genes mentioned above are involved in the organization of the extracellular matrix (ECM). ECM provides structure and support to the surrounding cells and is involved in differentiation, cell adhesion, and cell-to-cell communication. However, these genes do not explain all HCTD patients and many genes still await their discovery. Three typical examples of HCTD are Marfan syndrome (MFS), Ehlers-Danlos syndrome (EDS), and Loeys-Dietz syndrome (LDS). These syndromes show some degree of phenotypical overlap of cardiovascular, skeletal, and cutaneous features, although the dissection of the endophenotype allowed to address features specific for one syndrome rather than another. MFS is typically characterized by cardiovascular, ocular, and skeletal manifestations and is caused by heterozygous mutations in *FBN1*, coding for the extracellular matrix (ECM) protein fibrillin-1. The most common cardiovascular phenotype found in MFS are the aortic aneurysm and dissection at the sinuses of Valsalva. LDS is caused by mutations in *TGFBR1/2, SMAD2/3,* or *TGF*B*2/3*, all coding for components of the TGFβ-signaling pathway. LDS can be distinguished from MFS by the unique presence of hypertelorism, bifid uvula or cleft palate, and widespread aortic and arterial aneurysm and tortuosity.[8] Compared to MFS, LDS cardiovascular manifestations tend to be more severe. In contrast, no association is reported between LDS and the presence of ectopia lentis, a key distinguishing feature of MFS. Overlapping features between MFS and LDS include, scoliosis, pes planus, anterior chest deformity, spontaneous pneumothorax, and dural ectasia. EDS refers to a group of clinically and genetically heterogeneous connective tissue disorders and all subtypes are characterized by variable abnormalities of skin, ligaments and joints, blood vessels, and internal organs. Typical presenting features include joint hypermobility, skin hyperextensibility, and tissue fragility. Up to one quarter of the EDS patients show aortic aneurysmal disease. The latest EDS nosology distinguishes 13 subtypes.[8] Considerable phenotypic overlap is also observed between the different subtypes of LDS and EDS, respectively, which makes the clinical diagnosis difficult and highlights the importance of molecular diagnostic confirmation.

Hearing loss, isolated or syndromic, is another example of genetic heterogeneity facing difficulties in reaching the molecular diagnosis. Hearing loss is the most common congenital sensory impairment, affecting 1 in 500 newborns and 1 in 300 children by the age of four.[9] It is among the most heterogeneous conditions, and the most common causes of permanent congenital sensorineural and mixed hearing loss are congenital cytomegalovirus infection (CMV; 5%-20%), structural abnormalities of the temporal bones (30%- 40%), and genetic causes (50%).[10-11] Hereditary hearing loss and deafness can be regarded as syndromic or non-syndromic. Syndromic hearing impairment is associated with malformations of the external ear, with malformations in other organs, or with medical problems involving other organ systems and more than 400 genetic syndromes have been described.[12] Non-syndromic hearing impairment has not been associated with visible abnormalities of the external ear or any related medical problems; however, it can be associated with abnormalities of the middle ear and/or inner ear and more than 6,000 causative mutations have been identified in more than 110 genes. In both cases the most frequent genetic cause of congenital sensorineural hearing loss (SNHL) is disruptions of GJB2, the gene encoding Connexin 26 (Cx26), the major component of gap junctions in the cochlea.[13]

McKusick, in the article entitled "On Lumpers and Splitters, or the Nosology of Genetic Disease", published in 1969, asserts that "In genetic nosology both lumping and splitting have a place: lumping in connection with pleiotropism; splitting in connection with genetic heterogeneity"[1]. An approach is considered as "lumpers", when physicians prefer broader categories that include phenotypes sharing common features despite some differences; on the other hand, "splitters" prefer narrower categories, emphasizing variations rather than common features[1]. In this context, the genetic analysis by DNA sequencing was considered the final stage of the diagnostic process in patients, and diagnosis was made according to clinical manifestations and results of imaging and biochemical tests. However, genetic analysis by Sanger sequencing is a highly manual and time-consuming chemical process with a very low success rate, leading to problems in obtaining a diagnosis, as shown by a recent Australian study which observed that 30% of patients who finally received a molecular diagnosis had waited five or more years for their disease confirmation, 66% had consulted three or more doctors to obtain it and 46% had received at least one misdiagnosis.[14] The advent of next generation sequencing (NGS) has made it possible to analyze the entire coding heritage or the entire genome (exome) in a few days of work and has paved the way towards the identification of new molecular pathogenetic mechanisms.[15]

NGS has allowed a fast identification of pathogenetic mutations, and the number of new disease genes has grown exponentially from year to year (Fig. 1).[16] The possibility of sequencing and analysis of the entire coding heritage and of the whole genome has also "rewritten" many genetic conditions, from the etiological point of view.

The above-mentioned examples suggest two aspects very important: 1) the need for functional studies to make precise correlations between the altered function due to the variant with the resulting phenotype; 2) the “dissection” of the phenotype into endophenotypes, in order to find points of contact between apparently different diseases and on the contrary sharing the same molecular pathways. This approach is expected to rewrite entire chapters of human pathology by reclassifying many clinical conditions according to the underlying mechanism, paving the way to personalized medicine.

Precision medicine is expected to create diagnostic, prognostic, and therapeutic strategies precisely tailored to each patient’s requirements, providing patients with an appropriate treatment, with minimum adverse effects and maximum efficacy. In conclusion, the modification of the natural history of genetic pathologies up to their "correction" promoted by this new approach will lead to a deeper vision of genetic diseases which, until recently, are relegated mostly to a status of diseases diagnosable but not curable.

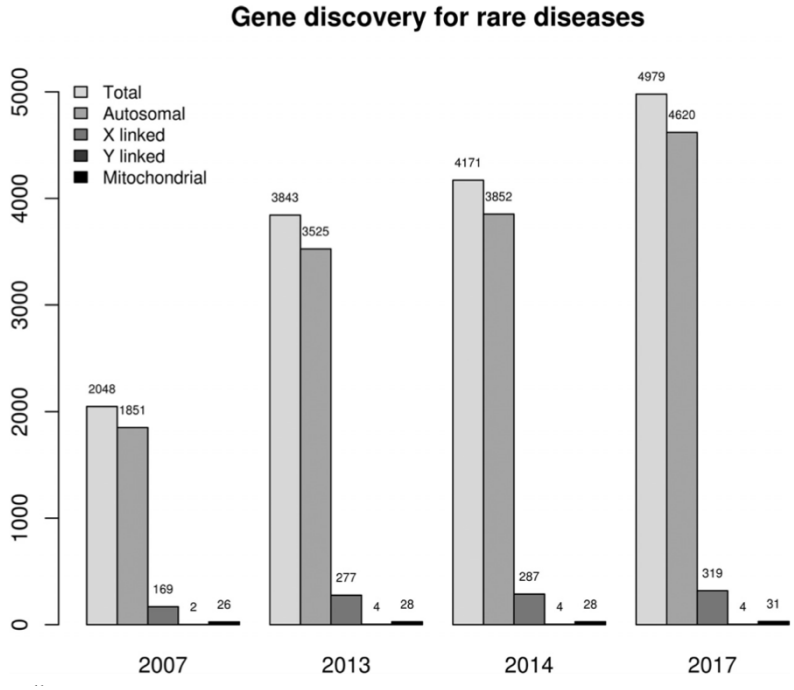

Figure. 1: Gene discovery for rare diseases

Chapter 1: Clinical and Genetic heterogeneity of Loeys-Dietz Syndromes

1. Introduction

During my PhD work I focused on the study of LDS, which represents a type of HCTD. LDS is an autosomal dominant disorder with a widespread involvement of different organ systems such as craniofacial (e.g., craniosynostosis), skeletal (joint laxity and contractures), integumental (skin hyperextensibility, dural ectasia) and ocular findings (e.g., strabismus).[17] The worst complication present in most of the patients affected by LDS and in general in subjects affected by some types of HCTD is the high risk of developing thoracic aortic aneurysms and dissection due to defects in the extracellular matrix composition which compromise the structural integrity of the aortic wall. Notably, thoracic aortic aneurysms have been reported in patients of all age groups, including young children.[18] Regarding the genetic alterations identified in LDS, about two thirds of mutations are de novo and one third is familial. All mutations causing LDS were found in genes involved in the TGF-*β* pathway, which regulates a variety of cellular processes including growth inhibition secondary to G1/S phase arrest, differentiation, apoptosis, immunosuppression, stimulation of connective tissue deposition, secondary induction of angiogenesis, and probably maintenance of genomic stability.[19] TGF-β induces these effects by activating the TGF-*β* receptor, a heterodimeric complex composed of type I (TGFBR1) and type II (TGFBR2) subunits, which are both serine-threonine kinases with single transmembrane domains.[19] Both TGFBRI and TGFBR2 appear to be essential for TGF-β induced effects on the cell.[19] The TGF-β receptor is activated through a sequence of events that is initiated by the TGFBR2 subunit binding to TGF-*β* ligand. The activated TGFBR2 associates with TGFBR1, and phosphorylates a glycine-serine rich sequence in TGFBRI. TGFBRI is then activated and can phosphorylate downstream targets.[19-20] The TGF-*β* receptor complex activates both the canonical signaling pathway, which includes SMAD2, SMAD3, and SMAD4, and the non-canonical signaling cascades (e.g. PI3K/AKT, p38-MAPK, MAPK-ERK, JNK, etc.) to produce the full spectrum of TGF-*β* responses.[19] LDS has been initially associated with mutations present in *TGFBR* genes, one-third of them have been identified in TGFBR1 (LDS1) whereas the remainder was found in TGFBR2 (LDS2).[21] Moreover, pathogenic variants were found in other four genes causing distinct, yet overlapping, LDS phenotypes nosologically classified as follows: *SMAD3* (LDS3), *TGFB2* (LDS4), *TGFB3* (LDS5), and *SMAD2* (LDS6).[22-23] Nowadays, different forms of LDS (LDS syndromes) appear to reflect genotype-phenotype correlations in terms of genes/variants associated with a prevalent phenotype.

For example, LDS patients with pathogenic variants in *SMAD3* displaying high frequency of osteoarthritis[24], whereas patients with variants in *TGFBR2* are strongly predisposed to develop cardiovascular problems.[24] It should be noted that a deeper genetic knowledge of mutated genes associated with more aggressive forms of the disorder is of paramount value for the correct management of patients and to plan appropriate prevention programs in clinical practice. In this context, my work focalized on two aims/ aspects.

The first year of this thesis was dedicated to LDS. First aim was to perform a retrospective multi-center study on clinical and mutational analyses in 24 novel LDS families with 34 patients. A systematic overview of LDS patients' features for each mutated gene was conducted to verify if observed genotype-phenotype correlations fitted current knowledge about mutations involved in LDS. Second aim of this study was the analysis of two atypical novel variants in *TGFBR1,* leading to the formation of prematurely truncated proteins in two unrelated LDS patients. In fact, looking at the molecular spectrum of *TGFBR1* mutations identified in literature, most of them are missense changes affecting residues located especially in the kinase domain, while a small part of them involves the receptor domain. Occasional small deletions, small insertions or gross insertions/deletions have been described. Surprisingly, almost all missense mutations are predicted to result in loss of kinase function of receptors[25] and lead to paradoxically upregulation of TGF-β signaling, causing chronic consequences such as an increased accumulation of phosphorylated SMAD2 in the aortic wall.[7-26] Of note, conversely nonsense mutations in *TGFBR1* have been shown to result in a distinct syndrome featuring skin cancer phenotype termed "multiple self-healing squamous epithelioma" (MSSE).[25]

In summary, we amplified the knowledge of genotype-phenotype correlations, in the context of LDS, by comparing our data with published studies. In addition, we described for the first time two novel variants in *TGFBR1* which escape nonsense-mediated mRNA decay (NMD) and lead to paradoxical upregulation of the TGFβ signaling pathway, thus contributing to the identification of a novel class of LDS disease-causative mutations.

1.1 Results-Aim 1

In this work we describe 34 patients from 24 families with 24 different variants in four distinct LDS-related genes identified in the proband of each family by direct sequencing. The majority of variants affected the *TGFBR1* (9/24) and *TGFBR2* (10/24) genes, four families showed variants in *SMAD3*, and 1 patient carried a *TGFB2* variant. No variants were identified in *SMAD2* and *TGFB3*. Fifteen variants affecting *TGFBR1*, *TGFBR2*, *SMAD3*, and *TGFB2* were novel, while nine in *TGFBR1*, *TGFBR2*, *SMAD3* were previously reported either in the literature or in the ClinVar database. Among the novel variants, 10 missense substitutions and one in-frame deletion altered two highly conserved amino acid residues p.(Lys232_Ile233del) in *TGFBR1* gene and were predicted to be pathogenetic by several *in silico* prediction algorithms. Moreover, the variants respected all the pathogenetic criteria reported in the American College of Medical Genetics and Genomics (ACMG) guidelines.[27] Likewise, the novel c.480del variant in *TGFB2* and the c.862_871+8del variant in *SMAD3* were classified as pathogenic by in silico prediction. Indeed, for the first variant, the prediction results in a frameshift and formation of a premature termination codon p.(Phe160Leufs*14) that probably activates nonsense-mediated mRNA decay (NMD). Concerning the other variant, the prediction results in an abnormal splicing since the canonical splice donor site is lost. Differently, for the c.263+6C>T variant in *TGFBR2* and the c.1009+1G>A variant in *SMAD3* we corroborated their pathogenicity demonstrating an effect on the splicing process on fresh blood samples. In detail, the first variant was classified as possibly pathogenic according to the ACMG, since it creates a new splice donor site 6 bases downstream of the wild-type donor with retention of 4 nucleotides of intron 3, formation of a stop codon (p.Arg114*) and activation of NMD. The second one was classified as pathogenic, since it abolishes the canonical splice donor site of exon 7 causing in-frame exon skipping (p.Arg292_Gly337del). So, a systematic overview of LDS patients' features for each mutated gene was conducted to verify if observed genotype-phenotype correlations fitted with data present in the literature. Overall, we confirmed a significant phenotypic overlap for *TGFBR1*/*2*, *SMAD3*, and *TGFB2* patients (Table 1), and we have better defined the prevalent phenotype associated with mutations in each gene.

Table 1. Comparison of the clinical features observed in previously reported and LDS patients described in this cohort for each distinct gene.

Clinical Features	*TGFBR1*		*TGFBR2*		*SMAD3*		*TGFB2*		*SMAD2*	*TGFB3*
	Lit.	This Cohort *n* = 12 (%)	Lit.	This Cohort *n* = 12 (%)	Lit.	This Cohort *n* = 9 (%)	Lit.	This Cohort *n* = 1	Lit.	Lit.
Hypertelorism	++++	10/12 (84)	++++	6/12 (50)	++	4/9 (44)	++	1/1	+	++
Strabismus	+	1/12 (8)	+	1/12 (8)	+	0/9	+	0/1	−	−
Malar hypoplasia	+++	8/12 (67)	+++	9/12 (75)	++	9/9 (100)	++	1/1	++++	++
Bifid uvula/Cleft palate	++++	3/12 (25)	++++	5/12 (42)	++	2/9 (22)	+	1/1	−	++
Dolichocephaly	+++	11/12 (92)	+++	7/12 (58)	+	3/9 (33)	−	0/1	++++	−
Hernia	+++	4/12 (33)	+++	6/12 (50)	++	5/9 (55)	++	1/1	++++	++
Striae	++	5/12 (42)	++	3/12 (25)	++	3/8 (37)	++	1/1	++	+
Pectus deformity	+++	5/12 (42)	+++	7/12 (58)	++	6/9 (66)	++	1/1	++	+++
Scoliosis	+++	10/12 (84)	+++	8/12 (67)	++	3/9 (33)	++	1/1	++	+++
Arachnodactyly	+++	5/12 (42)	+++	6/12 (50)	++	1/9 (11)	++	1/1	++	++
Talipes equinovarus	++	1/12 (8)	++	5/12 (42)	+	1/9 (11)	+	0/1	−	++
Osteoarthritis	++	0/11	++	0/10	++	3/6 (50)	+	0/1	++++	++
Cervical spine malformation/instability	+	1/11 (9)	+	2/9 (22)	+	0/3	−	1/1	−	+
Dural ectasia	++	1/11 (9)	++	3/8 (37)	+++	1/4 (25)	++	1/1	+	−
Mitral valve prolapse or insufficiency	++	5/12 (42)	++	7/10 (70)	++	5/9 (55)	++	1/1	++	++
Arterial tortuosity	++++	3/11 (27)	++++	5/11 (45)	++	1/6 (17)	++	1/1	+	+
Aortic root aneurysm	++++	12/12 (100)	++++	9/12 (75)	+++	7/9 (77)	+++	0/1	++++	++
Arterial aneurysms	+++	5/12 (42)	+++	5/11 (45)	+	2/9 (22)	+	0/1	+	+
Aortic dissection	++++	3/12 (25)	++++	2/12 (17)	++	1/9 (11)	+	0/1	−	++

Lit: Literature. Frequencies of clinical feature associated with LDS were scored as: − absent/infrequent; + <25%; ++ 25–50%; +++ 50–75%; ++++ >75%.

A major involvement of the cardiovascular system (ascending/aortic root aneurysm and mitral valve abnormalities) was found in all *TGFBR1/2* mutated patients; the only patient with a *TGFB2* pathogenic variant showed absence of aneurysms but revealed mitral valve prolapse and insufficiency, mild arterial tortuosity and varicose veins; three *SMAD3*-mutated families presented very mild cardiovascular anomalies, with only mitral valve prolapse registered in the proband and early osteoarthritis; the latter, considered as a hallmark of patients carrying mutations in *SMAD3*, was described only in one family, although segregated in the proband and in his father. Recurrent craniofacial dysmorphism such as hypertelorism, malar hypoplasia, micrognathia and highly arched palate, cleft palate and/or uvula, cutaneous features with translucent skin, striae and facial milia, hernias and skeletal manifestation like pes planus, pectus deformity, marfanoid habitus, and scoliosis are phenotypes present in all LDS patients. No mutations were identified in *SMAD2* and *TGFB3* genes. To date, 9 likely pathogenic variants in *SMAD2* have been described in 15 subjects displaying a broad range of features, including aneurysms, tortuosity of the entire arterial tree, and coronary artery dissections, even in the absence of prominent connective tissue characteristics.[28] Concerning *TGFB3*, 15 different variants were reported in 56 individuals presenting with phenotypic overlap between LDS and MFS.[29] In conclusion, our results show that cardiovascular phenotype is a prevalent alteration in the presence of mutation in *TGFBR1/2*, while the presence of mutations in other genes involved in TGFβ pathway results in mild cardiovascular disfunction.

1.2 Results-Aim2

1.2.1 Patients and clinical features

Family 1 consisted of two affected relatives, the proband (P1) and her father (P2). Family 2 consisted of a female proband (P3). The proband (P1) in family 1 was a 20-year-old-girl, second child of non-consanguineous parents. No anomalies were noted at birth. On physical examination, she presented with apparent ocular hypertelorism (Figure 2a, i), broad uvula with a median raphe. Her skin was velvety and slightly translucent with visible subcutaneous veins. Ocular features included high grade myopia. Musculoskeletal findings consisted of combined thumb and wrist signs. Since her father was affected by aortic aneurysm and dissections, she started serial echocardiographic examinations at a very young age, uncovering progressive aortic root dilatation, from the age of 14 years. Decreased bone mineral density was documented at dual-energy X-ray absorptiometry (DXA) scan at the age of 20 years. Five years later, echocardiography revealed trivial mitral valve regurgitation and a 40 mm aneurysm of the aortic root, also confirmed by total body magnetic resonance angiography (Figure 2a, ii-iii) for which she underwent successful valve-sparing aortic root and ascending aorta replacement with coronary arteries reimplantation (Figure 2a, iv). Involvement of other vascular districts (including coronary circulation) or vascular kinking were excluded.

Her father, P2, was the first child of healthy non-consanguineous parents. He was born at term with normal growth parameters, while neonatal course was characterized by cleft palate and bilateral inguinal hernia both surgically corrected before 1 year of age. His medical history was notable for early-onset aortic disease: aortic root aneurysm was first treated at the age of 10 years with aortic root replacement by means of a 25 mm homograft, while six years later the aortic valve was replaced with a Starr-Edwards mechanical valve for homograft dysfunction. At the age of 25 years, echocardiography revealed aortic arch aneurysm (70 mm) requiring total arch replacement. Starting from the age of 37 years, he underwent several surgeries, including descending thoraco-abdominal aortic replacement and aortic arch replacement for pseudoaneurysm at the site of previous surgical anastomoses. At the age of 41 years, computed tomography (CT) angiography showed tortuosity and elongation of the entire aorta and tight kinking of the descending aorta with thickening of the wall (Figure 2b, iii). Three years later, aortic arch dissection and aneurysmal dilatation of the left and right coronary were evident (Figure 2b, iv-v). Additional vascular findings included ectasia of both carotid artery bifurcations, abnormal course of both internal carotid arteries, anterior cerebral arteries with fusiform ectasia of the anterior communicating artery, tortuosity and elongation of both vertebral arteries and of the basilar arteries. DXA scan performed at the age of 42 years documented decreased

bone mineral density. On physical examination, at the age of 45 years, apparent ocular hypertelorism was noticed together with midline raphe of tongue and uvula (Figure 2b, i-ii). Orthopedic assessment was remarkable for low muscle bulk, pectus excavatum, severe scoliosis, limited hip external rotation, pes planus, and laxity of small joint. Cutaneous findings included facial milia, thin skin with visible subcutaneous veins and skin striae. The last CT angiography at 47 years documented aneurysmal dilatation of the partially thrombosed left ventricular apex of heart, worsening of the aneurysms and tortuosity of the entire aorta and its main side branches, dissection flap with eccentric parietal thrombotic apposition of the abdominal aorta aneurysm with the occlusion of the left renal artery (Figure 2b, vi). Paraseptal emphysema of the left middle pulmonary lobe was also present. Due to sudden rupture of the abdominal aorta aneurysm, he died at the age of 48 years. In family 2, the female proband (P3) was initially evaluated at the age of 7 months because of craniofacial dysmorphism. Family history was uninformative, but pregnancy had been obtained by assisted reproduction techniques and oocyte donation (no available data on the donor were available). On examination, length was 71 cm (97^{th} centile) and weight 7.2 kg (25^{th} centile). She displayed mild apparent ocular hypertelorism, triangular face, and highly arched palate. Arachnodactyly was particularly evident. Ophthalmological examination was normal. An echocardiography at the age of 3 years and 9 months showed normal anatomy, with a mild dilation of the aortic root (Z-score +2.27). Psychomotor development was initially reported as normal; however, at the age of 5 years she was diagnosed with attention deficit hyperactivity disorder. On re-evaluation at the age of 5 years and 7 months height was 113 cm (50^{th} centile) and weight 18 kg (10^{th} centile). Head circumference was 51 cm (+0.3 SD). She displayed mild hypertelorism with downslanting palpebral fissures, a long face with malar hypoplasia, pointed chin, high-arched palate (with normal uvula), and dental crowding. She had pectus excavatum and displayed strikingly long fingers of hands and feet, with palmar length 8 cm (75-97^{th} centile) and the middle finger 6.5 cm (>97^{th} centile).

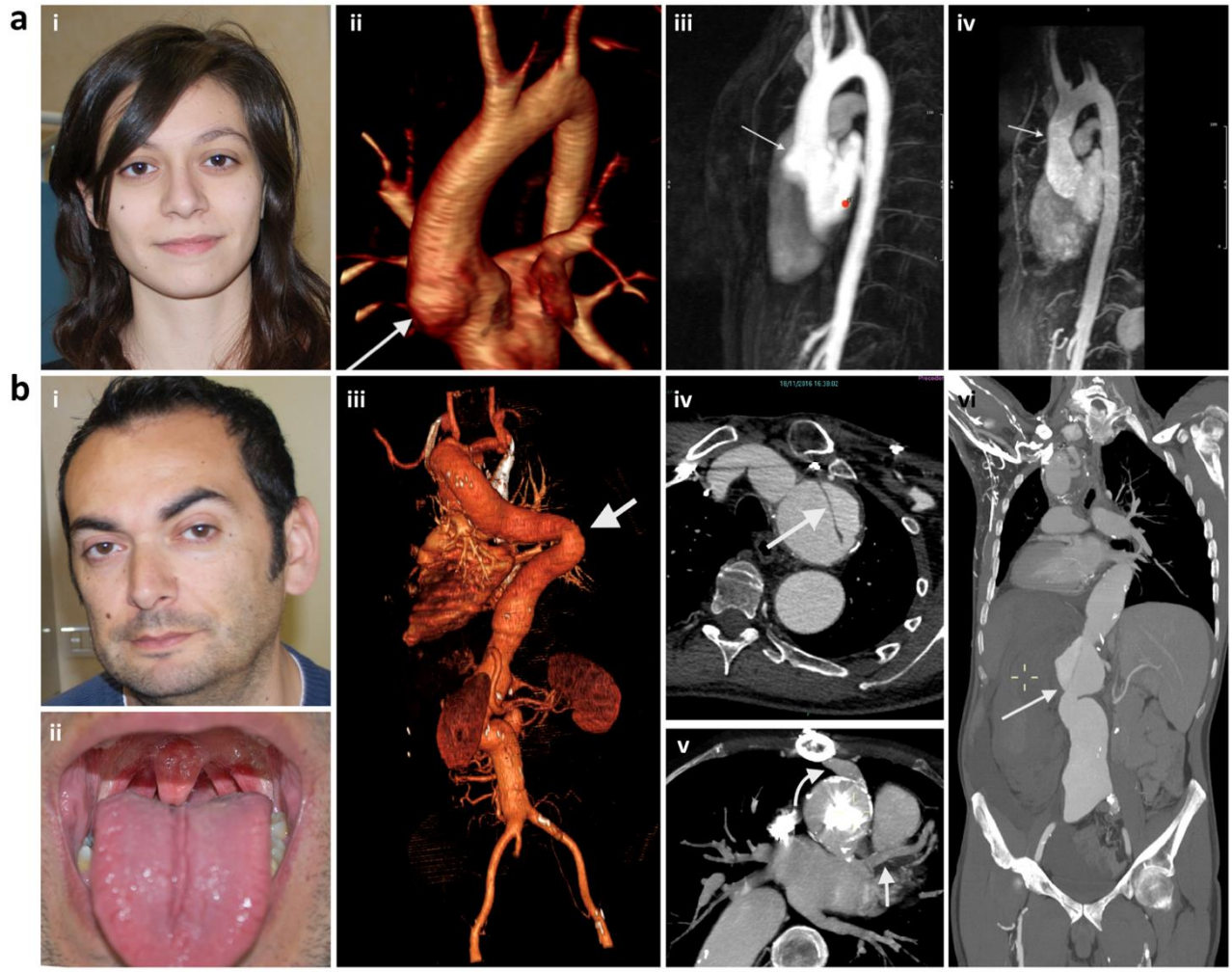

Figure 2. Clinical and instrumental findings in family 1. a) Patient P1 (proband). (i) Facial gestalt with hypertelorism at the age of 20 years. (ii-iv) Magnetic resonance angiographies performed at age 25 years showed aortic root dilatation before (ii and iii) and after surgery (iv). b) Patient P2. (i) Facial appearance with hypertelorism at the age of 45 years, (ii) midline raphe of tongue and uvula. (iii-vi) Total body computed tomography angiographies documented tortuosity of the entire aorta and tight kinking at age 41 years (iii), dissection of the aortic arch (iv), left and right coronary dilatation (v, straight and curve arrows, respectively) at 44 years, extension of the dissection at age 47 years with involvement of supra-aortic branches and abdominal aorta (vi) and left renal occlusion (arrow).

1.2.2 Genetic analysis

In view of the patient's phenotype, highly suggestive of a syndromic heritable thoracic aortic disease, a custom NGS panel was run including all LDS-associated genes and those of overlapping disorders. The heterozygous c.1342dup variant and the heterozygous c.1335_1338del variants were identified in *TGFBR1*, respectively from family 1 and family 2, and subsequently confirmed by Sanger sequencing (Figure 3). The relatives of both families did not show the pathogenetic variants. The variants were located in exon 8 and both were predicted to cause a translational frameshift and a premature stop codon. The c.1342dup and c.1335_1338del variants had not been previously reported in the literature and were absent from all following-listed databases: dbSNP, gnomAD, Genome of the Netherlands, Montalcino Aortic Consortium, LOVD and HGMD.

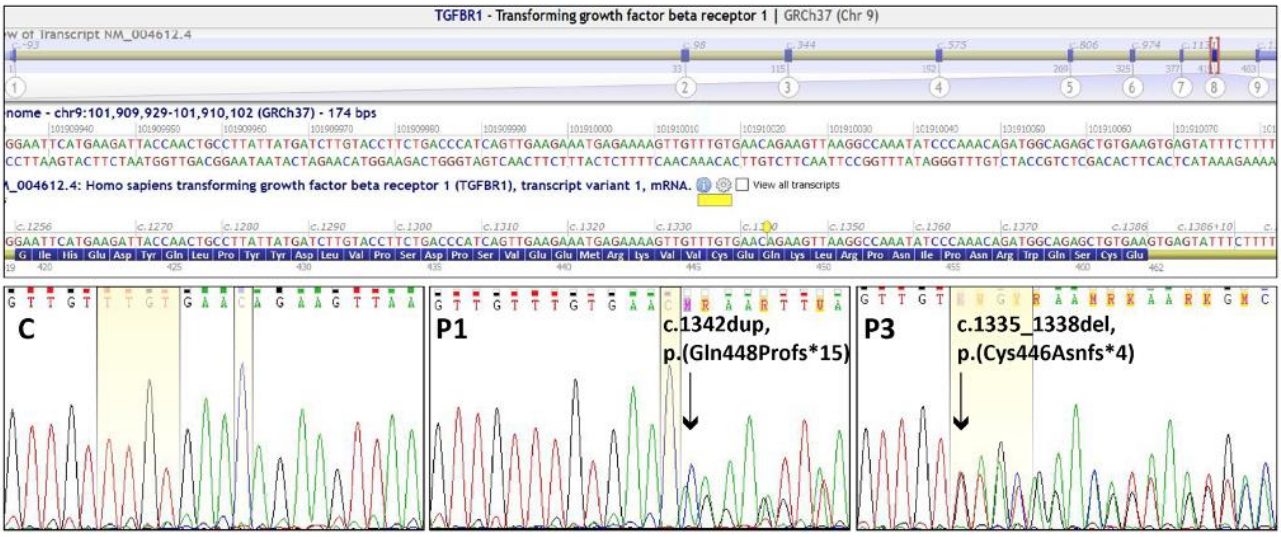

Figure 3. Genetic analysis. View of exon 8 of *TGFBR1* (NM_004612.4, NP_004603.1) with the Alamut Visual 2.15 software showing the near positions to the c.1342dup, p.(Gln446Profs*15) (yellow circle) and c.1335_1338del, p.(Cys446Asnfs*4) (yellow box) frameshift variants identified by NGS panels in P1 and P3, respectively. Sanger sequencing and segregation analysis confirmed the presence of the c.1342dup variant in the proband of family 1 (P1) and in her father (P2, not shown), and of the c.1335_1338del variant in the proband of family 2 (P3), which was absent in her father (C).

1.2.3 Search for similar TGFBR1 variants in available databases

In the ClinVar database, an identical c.1342dup variant was mentioned (RCV001209677.2), classified of uncertain significance and associated to a "familial case of thoracic aortic aneurysm and dissections" without further information. In the same database, another very closely located and similar variant c.1302_1303dupTG in *TGFBR1* exon 8 (RCV000243082.2), leading to a frameshift and prematurely truncated protein p.(Asp435Valfs*8) was also classified of uncertain significance and associated with an unspecified "cardiovascular phenotype".

1.2.4 Bioinformatics and functional analyses

We first performed transcript analysis on cDNA from blood lymphocytes of patients P1 and P3 by assessing the relative abundance of the wild-type (wt) and mutant transcripts through deep sequencing of a 593 bp fragment encompassing both variants, thus demonstrating that both mutant alleles escaped NMD. Biallelic expression was also confirmed by Sanger sequencing of an RT-PCR product on cDNA obtained from patient's P2 dermal fibroblasts. Both p.(Gln448Profs*15) and p.(Cys446Asnfs*4) variants are predicted to result in truncated proteins within the STK domains lacking the last 43 and 56 amino acid residues, respectively. The architecture of the cytoplasmatic kinase domain characterized by a N-terminal lobe (N-lobe), where the ATP binding and catalytic site lies, and a C-terminal lobe (C-lobe) associated with kinase activity regulation. Three alpha helices G, H, and I at the C-lobe constitute the GHI helical sub-domain, which is conserved in all the eukaryote protein kinases (EPKs). In general, this sub-domain regulates the kinase activity of the N-lobe by allosteric control, the oligomerization status, and the interaction with macromolecular substrates.[30-31] As shown in Figure 4, 3D modeling of the truncated variants p.(Gln448Profs*15) and p.(Cys446Asnfs*4) displayed that the mutants completely miss this motif and that the loss of the GHI helical subdomain disrupts the interconnection between the C-lobe and the N-lobe. Indeed, the two mutated proteins lack a conserved, crucial salt-bridge (E382-R482), thus probably altering the phosphorylating activity.

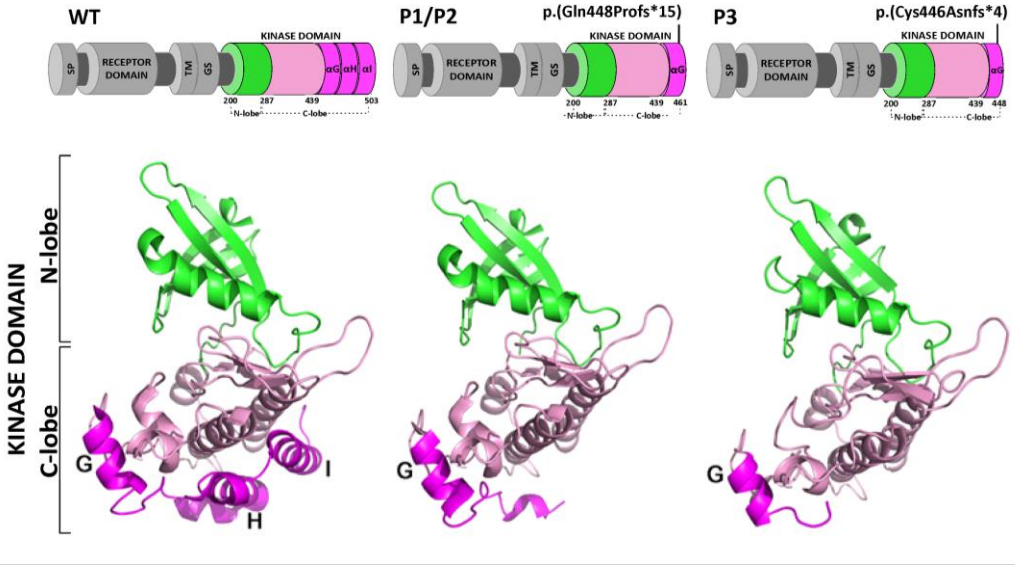

Figure 4. Bioinformatics studies a) Protein structure modelling of the TGFβR1 kinase domain variants. Above, schematic representation of the wild type (wt) TGF-beta receptor type-1 (TGFβR1) protein as compared to the truncated forms identified in this study lacking respectively the last 43 and 56 amino acid residues (SP: signal peptide, TM: transmembrane domain, GS: glycine- and serine-rich sequence domain). Below, cartoon representation of the 3D structures of the cytoplasmatic kinase domain of the TGFβR1 protein variants described in this study. On the left, the wt structure (residues 200-503; PDB code: 1VJY) is shown, while the 3D models of the p.(Gln448Profs*15) and p.(Cys446Asnfs*4) variants are displayed in the middle and on the right, respectively. The N-terminal lobe (residues 200-286) and the C-terminal lobe (residues 287-503) are displayed respectively in green and pink cartoons for each protein, while the GHI helical subdomain (residues 439-503), which is almost completely lost by the both mutants, belonging to the C-terminal lobe is shown in magenta.

Western blot analysis (WB), performed with three different antibodies directed to distinct regions of the TGFβR1 protein, failed to reveal the truncated form of the receptor in total protein extracts. Interestingly, densitometric analysis showed that full-length TGFBR1 protein levels were not significantly reduced in patient P2's cells (Figure 5a). Canonical TGFβ signaling pathway, explored in patient's P2 dermal fibroblasts by immunofluorescence microscopy (IF), revealed SMAD2 activation under steady-state culture conditions. Both total SMAD2 and its phosphorylated form were present at significantly higher levels in the cytoplasm and nuclei as compared to control fibroblasts (Figure 5b). Concerning non-canonical TGFβ signaling, IF showed augmented levels of phosphorylated p38-MAPK (p-p38) in the patient's cells' nuclei as compared to control cells. WB on whole cell extracts revealed an approximately 7.5-fold increase ($p < 0.001$) of the phospho-p38/p38 ratio in patient's cells as compared to control cells, thus confirming increased p38 activity (Figure 5c). In addition, non-canonical ERK-mediated TGFβ signaling was analyzed by WB which revealed a 1.6-fold increase ($p < 0.05$) of the phospho-ERK/ERK ratio (Figure 5c), suggesting ERK1/2 activation in patient's cells. Consistent with the role of TGFβ signaling as a potent driver of fibroblast-to-myofibroblast transition, α-SMA was improved in patient's cells (about 30%), while control cells showed diffuse staining in the cytoplasm and perinuclear region (Figure 4b). WB analysis confirmed an about 5-fold increase ($p < 0.001$) of α-SMA levels in patient's fibroblasts as compared to control cells, in line with increased myogenic differentiation in LDS fibroblasts (Figure 5b, c).

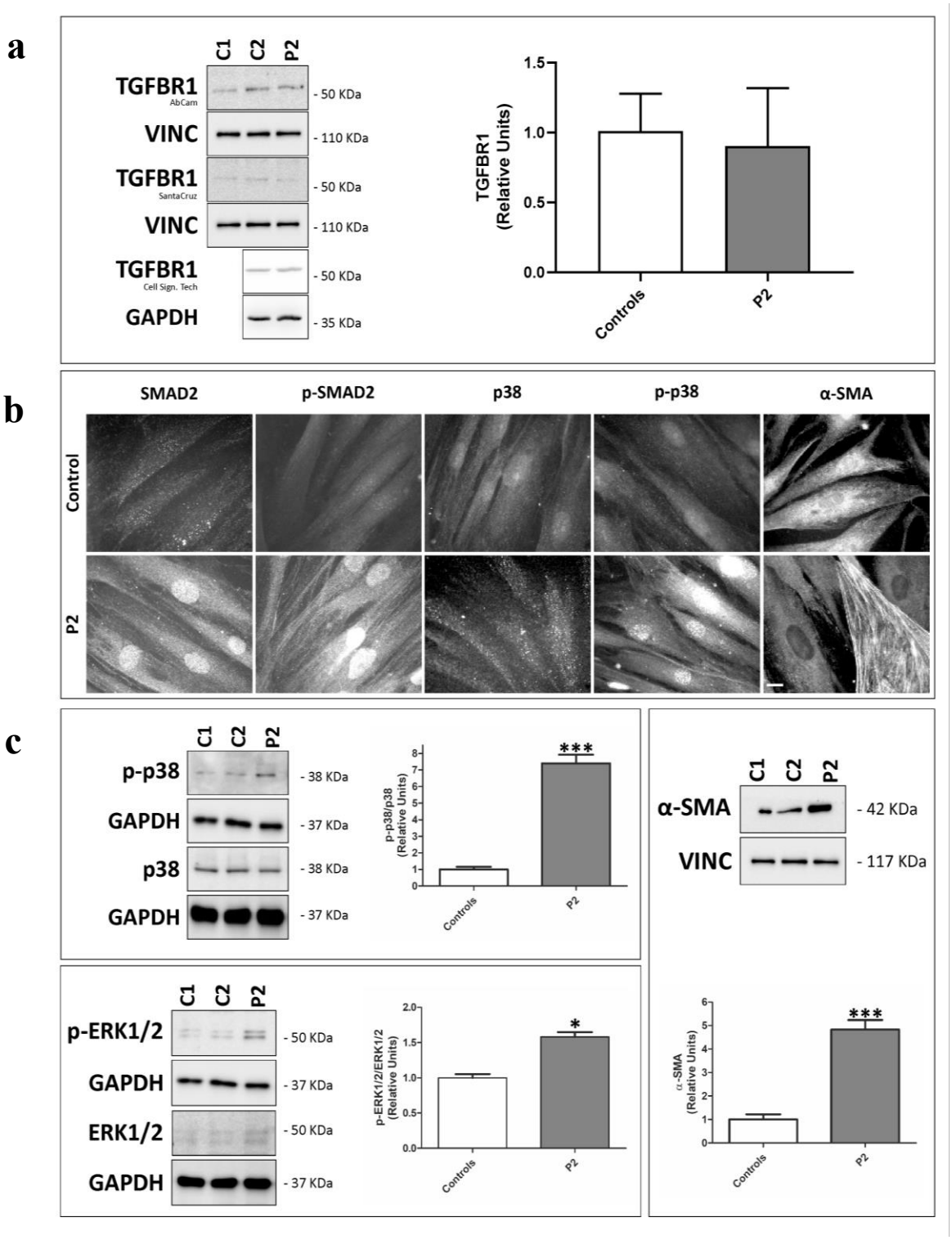
a
C1
C2
P2
TGFBR1
AbCam
- 50 KDa
VINC
- 110 KDa
TGFBR1
SantaCruz
- 50 KDa
VINC
- 110 KDa
TGFBR1
Cell Sign. Tech
- 50 KDa
GAPDH
- 35 KDa
TGFBR1 (Relative Units)
1.5
1.0
0.5
0.0
Controls
P2
b
SMAD2
p-SMAD2
p38
p-p38
α-SMA
Control
P2
c
p-p38
- 38 KDa
GAPDH
- 37 KDa
p38
- 38 KDa
GAPDH
- 37 KDa
p-p38/p38 (Relative Units)
***
Controls
P2
α-SMA
- 42 KDa
VINC
- 117 KDa
p-ERK1/2
- 50 KDa
GAPDH
- 37 KDa
ERK1/2
- 50 KDa
GAPDH
- 37 KDa
p-ERK1/2/ERK1/2 (Relative Units)
*
α-SMA (Relative Units)
***

Figure 5. Molecular and cellular studies. a) Illustrative images of WB results for TGFBR1 performed on fibroblasts from patient P2 and two healthy donors (C1, C2) with three different antibodies directed to distinct TGFBR1 regions: a mouse monoclonal antibody directed to aa 26-125 (SantaCruz); two rabbit polyclonal antibodies directed to aa 150-250 and the central intracellular region (AbCam and Cell Signaling Technology, respectively). Vinculin (VINC) and GAPDH were used as internal loading control for normalization. The graph shows quantitative results (presented as fold change) of the TGFBR1 levels achieved from 6 independent experiments, which revealed no significant differences between patient's and control cells. Error bars represent the mean value ± SD. b) IF of SMAD2 and its phosphorylated form (p-SMAD2; pS465/S467), p38 and its phosphorylated form (p-p38, pT180/Y182), and of α-SMA demonstrated enhanced canonical and non-canonical TGFβ signaling and partial α-SMA cytoskeleton organization (about 30% of positive cells) in patient P2 dermal fibroblasts as compared to controls (C). The experiments were repeated three times and images of control cells are representative of two different cell strains; scale bar: 8 μm. c) Illustrative images of WB results for ERK1/2 and p-ERK1/2 (pT202/Y204), p38 and p-p38 (pT180/Y182), and α-SMA performed on fibroblasts from patient P2 and two healthy donors (C1, C2). GAPDH and vinculin (VINC) were used as internal loading control for normalization. The graphs show quantitative results (presented as fold change) of the p-ERK1/2/ERK1/2 ratio, p-p38/p38 ratio, and α-SMA levels achieved from 3 independent experiments, which confirmed increased TGFβ signaling and α-SMA levels in patient's cells. Error bars represent the mean value ± SD (*$p < 0.05$; ***$p < 0.001$).

1.3 Discussion

TAAD is the worst manifestation of several HCTD (such as MFS, LDS, vascular form of EDS, arterial tortuosity syndrome[24]), and the identification of mutated genes and thus biological pathways involved in these syndromes is of paramount importance for the management of the patients and for the development of personalized medicine. Genetic testing guides management strategies to enable better outcomes for patient mortality and morbidity. Study of the specific genotype may suggest the appropriate timing of aortic repair and allows for screening of at-risk family members.[32] For this purpose, over the past decade NGS analysis led to the identification of genes involved in the HCTD, thus allowed to set up NGS panels for screening in order to address correct diagnosis, early treatment strategies, and appropriate follow-up in mutated individuals. Importantly, association studies are required to provide relevant information about the distribution and the nature of gene variants that may significantly influence age of onset, severity, and clinical penetrance of genetic disorders allowing a risk stratification analysis. Deciphering of the genotype-phenotype correlations and, more in deep, the correlation between variants and severity of the disease, is a major goal of human genetics since early interventional strategies may prevent life-threatening complications. Literature data already provided a general indication about the spectrum of disease severity for LDS, from the most to the least severe form: LDS1=LDS2>LDS3>LDS4>LDS5.[33] My work had the purpose to broaden the clinical and molecular spectrum of LDS, corroborating and expanding previously delineated genotype-phenotype correlations. The first part of my work (aim 1) confirmed that patients with mutations in *TGFBR1/2* have a major involvement of cardiovascular system, whereas a mild cardiovascular feature was observed with mutations in *SMAD3* and *TGFB2* genes. Moreover, we identified new variants in LDS genes and summarized the clinical data of these patients, especially their vascular phenotypic data, which could provide further refinement of our knowledge of LDS. Therefore, additional clinical and genetic data on LDS from around the world should be collected and analyzed hopefully to define gene-specific vascular treatment guidelines for LDS, rather than treat them all with the same approach.

In the second part of my work (aim 2), it was observed for the first time the involvement of two truncating variants in the *TGFBR1* gene involved in the onset of the LDS. To note, such variants are predicted to cause TGFBR1 haploinsufficiency, archetypical of MSSE rather than LDS. Interestingly, the data show that the frameshift mutation found in our patients, in the same way as the missense variants, leads to paradoxical TGFβ signaling accordingly with the LDS phenotype. Even though it has not been possible to reveal the truncated form of the receptor by WB but observing normal levels of full-length TGFBR1 protein, an hyperactivation of TGFβ pathway in the absence of stimulation

was evident in the patient's cells. In addition, we observed an increased level of α-SMA in fibroblast and considering that a high level of this protein is common to all syndromic and non-syndromic aortic diseases[17], we can assert that the above-mentioned variants are involved in aneurysm development. Anyway, both our newly reported variants, together with two similar alterations listed in the ClinVar database, were classified as variants of uncertain significance according to current guidelines[22]. In conclusion, we expanded the allelic repertoire of *TGFBR1* gene mutations associated with LDS including truncating variants, and we demonstrated the pathogenicity of the new two variants by functional study, highlighting the importance of clinical genetic databases integrated with functional data for the correct interpretation of genomic variants.

1.4 Material and Methods

1.4.1 Genetic investigation

Molecular analyses of patients P1 and P2 were achieved in the laboratory for genetic testing at the Division of Biology and Genetics, Department of Molecular and Translational Medicine, of the University of Brescia. Genetic testing was performed on genomic DNA purified from peripheral blood leukocytes by standard procedures. The proband P1 was characterized by using an in-house amplicon based NGS panel and the IonTorrent platform. Briefly, two panel pools of the custom "connective tissue panel – CTP" (*TGFBR1, TGFBR2, SMAD3, TGFB2, TGFB3, SMAD2 (LDS types 1-6), ABCC6, ACTA2, ADAMTS2, B3GALT6, B4GALT7, CBS, CHST14, COL1A1, COL1A2, COL3A1, COL5A1, COL5A2, DSE, FBN1, FKBP14, FLNA, MED12, MFAP5, MYH11, MYLK, NOTCH1, PRKG1, SLC2A10, SMAD4, SLC39A13*) were generated with the AmpliSeq Designer tool (Thermo Fisher Scientific). Panel libraries were produced using the AmpliSeq Library kit 2.0, which includes reagents for generating amplicons with the Ion AmpliSeq primers and the Ion Xpress™ barcode adapters, following manufacturer's protocols (Thermo Fisher Scientific). Library template preparation was performed with the Ion 520 & Ion 530 kit – OT2 on the Ion OneTouch 2 instrument and sequenced on the Ion S5 instrument with the Ion 520 chip, as previously reported.[30] Basecalling and sequence alignment against hg19 genome assembly were performed with the Ion Torrent Suite software v.5.0.2 and genetic variants were identified by the Ion Torrent Variant Caller v.5.0.2.1. Further evaluations, including copy number variation (CNV) analysis, were performed with the Ion Reporter software 5.6.

Whole exome sequencing was performed in P2 using the Ion Proton platform and the AmpliSeq Exome RDY kit for library preparation following manufacturer's protocols (Thermo Fisher Scientific Inc.). Briefly, libraries template preparation was achieved using the Ion PI Hi-Q OT2 200 kit on the Ion OneTouch 2 and sequencing run was performed with the Ion PI Hi-Q Sequencing 200 kit. The templated Ion Sphere Particles (ISP) were enriched for positive ISP using the Ion OneTouch ES and sequenced on Ion Proton with the Ion PI chip v3. Basecalling and sequence alignment against hg19 genome assembly were performed using Ion Torrent Suite software 5.16, and genetic variants were identified using Torrent Suite Variant Caller pipeline 5.16. Variants were decomposed and normalized using vt tool,[31] filtered for quality as previously reported[32] and by using GARFIELD-NGS,[33] and annotated using ANNOVAR.[34] Variants were filtered according to the following criteria: i) minor allele frequency (MAF) < 0.01 in 1000G and GnomAD v2.1.1 databases; ii) predicted to alter protein product, namely missense, stop-affecting or splice-affecting variants; iii) not present in

our internal database of WES experiments (n > 500); iv) not classified as (likely) benign in the ClinVar database (https://www.ncbi.nlm.nih.gov/clinvar/). Filtered variants were prioritized based on their CADD,[35] DANN,[36] and M-CAP[37] scores to retain most likely deleterious variants. RVIS[38] and GDI[39] scores were then used to rank more intolerant genes.

Molecular analysis of patient P3 was achieved in the Laboratory for Genetic Testing, Clinical Genetics Unit, Department of Women and Children's Health, University of Padova. NGS of genomic DNA purified from peripheral blood leukocytes was carried out by using a custom-made Agilent HaloPlex HS kit (genes: *ACTA2*, *COL3A1*, *FBN1*, *FOXE3*, *LOX*, *MFAP5*, *MYH11*, *MYLK*, *PRKG1*, *SMAD3*, *TGFB2*, *TGFB3*, *TGFBR1*, and *TGFBR2*) on a MiSeq sequencer (Illumina). Data analyses, including CNV analysis, were performed using the Agilent SureCall software, as previously reported.[40] Specific parameters are available upon request.

To exclude other possible variants contributing to the phenotype, Clinical Exome analysis was performed, using TrusightOne Expaned Kit (Illumina) and a NextSeq 550 sequencer (Illumina), according to the manufacturer's protocols. We initially excluded variants with read depth (RD) <10 or alternate allele (ALT) variant frequency (VF) <20% and known artefacts (from our internal database). For potentially recessive defects, we excluded variants with MAF ≥ 1%, and then variants in genes harboring a single heterozygous variant.

We considered only functional variants (missense, stop- or splice-affecting, and CDS indels) and excluded variants found in homozygosity in healthy controls (gnomAD 2.1 and 3.1). For potentially dominant defects, we excluded variants with MAF ≥ 0.01%, we included only functional variants (missense, stop- or splice-affecting, and CDS indels) and excluded those present in our internal database. Finally, we excluded single variants in known recessive genes.

Both *TGFBR1* (NM_004612.4; NP_004603.1) novel variants were confirmed by Sanger sequencing on an ABI 3100XL Genetic Analyzer (Applied Biosystems) and electropherograms were analyzed with the Sequence Scanner 2.0 software (Applied Biosystems). The variants nomenclature was generated with the Alamut 2.5 software (Interactive Biosoftware, Sophia Genetics) and variants were reported following the guidelines of the Human Genome Variation Society (HGVS, http://www.hgvs.org/mutnomen).

1.4.2 Skin biopsy and cell cultures

Primary fibroblasts were established from a skin biopsy of patient P2 and two age- and sex-matched healthy donors by standard protocol. Briefly, a 3 mm-punch arm biopsy was deprived of the epidermis, mechanically dissected and the dermis fragments were set up under a coverslide in the presence of Earle's Modified Eagle Medium (MEM) supplemented with 2 mM L-glutamine, 100

μg/ml penicillin and streptomycin, and 20% FBS (Life Technologies) at 37 °C in a 5% CO_2 atmosphere. After 3–4 weeks, confluent cells were harvested by 0.25% trypsin/0.02% EDTA treatment and expanded. Secondary cell cultures were grown in the presence of MEM supplemented with 10% FBS. Cells were analyzed between 2nd and 4th *in vitro* passage.

1.4.3 Immunofluorescence microscopy

To investigate SMAD2 and its Ser465/467 phosphorylation, fibroblasts derived from patient P2 and two healthy donors were grown on glass cover slides at 37°C in a 5% CO_2 atmosphere for 72 h. Cells were fixed 7 min in 3% PFA/60 mM sucrose, permeabilized for 1 min and 45 sec in 0.5% (v/v) Triton X-100 and reacted for 2 h respectively with 1:300 anti-SMAD2 monoclonal Ab (mAb) (Cell Signaling Technology, clone 86F7) and with 1:100 rabbit anti-phospho-SMAD2 (Ser465/467) Ab (Cell Signaling Technology, #3101). The analysis of p38 MAPK and its Thr180/Tyr182 phosphorylation was performed on cells fixed in cold methanol, permeabilized for 1 h with 0.5% (v/v) Triton X-100, and immunoreacted respectively with 2.5 μg/ml anti-p38 MAPK mAb (Abcam, clone M138) and 5.0 μg/ml rabbit anti-pT180/Y182-p38 MAPK Ab (Abcam, # ab4822). To evaluate the α-smooth muscle actin (α-SMA) cytoskeleton organization, cells were fixed in cold methanol and reacted for 1 h with 1 μg/ml anti-α-SMA mAb (Sigma Chemicals, Clone 1A4). After washing in PBS 1x, cells were reacted for 1 h with the Alexa Fluor®488 anti-rabbit and Alexa Fluor®594 anti-mouse IgGs (Thermo Fisher Scientific, #A32731 and #A32742, respectively). IF signals were acquired by a CCD black-and-white TV camera (SensiCam-PCO Computer Optics) mounted on a Zeiss fluorescence Axiovert microscope and digitalized by the Image Pro Plus software (Media Cybernetics). The experiments were repeated three times.

1.4.4 Western blotting

To analyze protein expression in cultured dermal fibroblasts, cell extracts of patient P2 and two healthy donors were prepared on ice with RIPA buffer (Tris–HCl pH 8, 50 mM, NaCl 150 mM, sodium deoxycholate 0.5%, sodium dodecyl sulphate (SDS) 0.1%, NP40 1%, NaF 50 mM, sodium orthovanadate 10 mM, protease inhibitor cocktail from Roche). Protein concentration was determined using Bio-Rad Protein Assay Dye Reagent Concentrate (Bio-Rad, #5000006). Proteins were loaded in equal amounts on 10%-15% SDS polyacrylamide gels (SDS–PAGE) and transferred to nitrocellulose membranes (Hybond-C, GE Healthcare). After transfer, membranes were blocked for 1 h in 5% BSA/TTBS (20 mM Tris–HCl, pH 7.5, 500 mM NaCl, 0.05% Tween 20). The desired proteins were detected by incubating overnight at 4 °C with the following primary antibodies in 5% BSA/TBS: rabbit anti-phospho ERK1/2 Ab (T202/Y204) (Thermo Fisher Scientific, #MILAN8R,

used at 1:1000), rabbit anti-ERK1/2 Ab (Thermo Fisher Scientific, #13-6200, used at 1:500), rabbit anti-phospho p38 (T180/Y182) Ab (Cell Signaling Technology, #9212, used at 1:500), rabbit anti-p38 MAPK Ab (Abcam, cat. #ab4822, used at 1:500), mouse anti-α-SMA mAb (Sigma-Aldrich, #A2547, used at 1:500), rabbit anti-GAPDH Ab (Santa Cruz Biotechnology, #sc-25778, used at 1:1000), mouse anti-vinculin mAb (Santa Cruz Biotechnology, #sc-73614, used at 1:1000), rabbit anti-TGFBR1 Ab (abcam, #ab31013-500), mouse anti-TGFBR1 Ab (Santa Cruz Biotechnology, #sc-130348), rabbit anti-TGFBR1 Ab (Cell Signaling Technology, #3712S) . After incubation with primary antibodies, each membrane was washed 5 times with 1x TTBS for 15 min at room temperature. Subsequently, membranes were incubated with 1:10.000 diluted HRP-conjugated secondary antibodies (GE Healthcare, anti-mouse #NA931V and anti-rabbit #NA934V) in 5% BSA/TTBS for 1 h at room temperature. Antibody binding was detected with the ECL plus detection system (GE Healthcare) and acquired with ChemiDoc Touch Imaging System (Bio-Rad Laboratories). The densities of the specific bands were quantified and normalized with GAPDH and vinculin as internal loading control by using the Image Lab software (Bio-Rad Laboratories). The relative expression values of p-ERK1/2/ERK1/2 and p-p38/p38 ratios, and of α-SMA were normalized to “1” in control cells (mean of two different cell strains), and then the corresponding expression fold changes were calculated in three independent experiments. Statistical analysis and graphs were obtained with the GraphPad Prism 8.0.2 software according to unpaired two-tailed student’s t-test and considering a p-value of less than 0.05 as significant; error bars in the graphs were generated using ± SD.

Chapter 2: RIPK4 regulates cell-cell adhesion in epidermal development and homeostasis

2. Introduction

Genetic heterogeneity can result in overlapping phenotypes, as in the case of genodermatoses such as distinct forms of EDs. Indeed, features such as cleft lip and/or palate, oral synechiae, pterygia and syndactyly have been observed in patients carrying pathogenic variants in *Tumor proteion 63 (TP63)* or *Interferon regulatory factor 6 (IRF6*) or *Poliovirus receptor-related protein 4* (*PVRL4)* genes.[34-35] Biallelic variants in *Receptor-interacting protein kinase* (*RIPK4)* also cause a genetic syndrome characterized by ectodermal derivates defects, variably associated to craniofacial (ankyloblepharon, cleft lip and/or palate, oral synechiae), limbs (pterygia), and/or genital anomalies.[36] Distinct mutations in *RIPK4* are associated with clinical variability ranges from an early lethal phenotype observed in Bartsocas-Papas syndrome (BPS or autosomal recessive Popliteal Pterygium Syndrome - PPS; OMIM#263650) [37-38], to the milder form termed Curly Hair, Ankyloblepharon, and Nail Dysplasia (CHAND; OMIM#214350).[39-40] RIPK4 is a member of the RIP serine/threonine kinase family, widely expressed in embryonic and mature tissues and key regulators of cellular response, host defense and skin barrier integrity.[41] Structurally, RIPK4 is organized in two domains: the highly conserved N-terminal region, composed of a catalytic N-lobe and regulatory C-lobe; and the C-terminal region, consisting of a protein-protein interaction domain with 12 ankyrin repeats, which modulate RIPK4 function and specificity. RIPK4 exists in three distinct forms: underphosphorylated, phosphorylated and hyper-phosphorylated. The protein is initially synthesized as an underphosphorylated soluble form that is quantitatively converted to a detergent-soluble protein, at least in part, by the intrinsic catalytic activity of kinase domain itself.[42] Through its kinase activity, RIPK4 phosphorylates IRF6, leading the latter to nuclear translocation and trans-activator function. To note, RIPK4 and IRF6 were known to operate in the same biological processes important for the induction of keratinocyte differentiation.[43]

In turn, their expression, together with that of several components of junctional complexes, is controlled by p63, the master regulator of epidermal development.[44-45]

In this work we characterized two siblings seen in our disease outpatient clinics and seeking for a genetic diagnosis of their disorder. They showed novel biallelic mutations in *RIPK4* leading to a distinct EDs dominated by hair and nail anomalies, cutaneous syndactyly and hyperkeratosis a phenotype similar to that observed in patients with mutation in *PVRL4*. So, the aim of this study was to show the pathogenetic effect of these two new variants and to decipher the etiopathogenetic

mechanism underlying the clinical convergence of the phenotypes derived from mutations in *RIPK4*, *PVRL4* and observed in EDs.

2.1 Results

2.1.1 Patients and genetic analysis

The proband is a male individual seen at 32 years of age displaying early scalp alopecia, sparse, curly and brittle hair with tendency to break. At birth, cutaneous syndactyly affecting digits 3-4 was evident, while he was told by his parents to be born with closed eyes and that the thin line of skin that joined the eyelids had been surgically removed at birth. His younger sister, seen at age of 27 years, suffered from an overlapping phenotype dominated by abnormal, brittle, uncombable and sparse hair, nail dysplasia and cutaneous syndactyly of hands and feet. Her nose was large with broad base and distinctive pseudo-cleft starting from the nostrils were evident. The skin was thin and dry with hyperkeratosis observable at the skin folds of the hands and at the soles (Figure 6). The siblings were born from non-consanguineous healthy parents. Based on the patients' clinical manifestations compatible with EDs, in particular with Ectodermal Dysplasia Syndactyly Syndrome (EDSS1, OMIM#613573), *PVRL4* gene was first analyzed by Sanger sequencing, and disease-causative mutations were excluded. Since the EDs show a spectrum phenotypic resulting from mutations in several genes, we decided to carry out a clinical exome sequencing in order to generate datasets from constitutive DNAs of both affected siblings and identify variants in known disease-causative genes. The variant filtering process led to the identification of 37 single nucleotide variations shared by the siblings in 9 distinct genes, including two heterozygous missense variants in the *RIPK4* gene (NM_020639.2): c.722G>A (p.Arg241His) in exon 5 and c.1283C>T (p.Pro428Leu) in exon 8 (Figure 7). These two variants were classified as damaging/deleterious by a variety of prediction algorithms, including PolyPhen, SIFT and Provean. Sanger sequencing confirmed the inheritance of the c.722G>A and c.1283C>T variants from their mother and father, respectively. Neither change affected exon splicing as witnessed by normal exon 5 and exon 8 amplification by reverse transcriptase (RT)-PCR analysis of the RNA purified from patient cultured keratinocytes.

Figure 6. Clinical findings in *RIPK4* mutated sibs. Clinical and histological presentation of the affected siblings. Upper panels, images from the proband, lower panels from the younger sister, showing early alopecia with sparse, curly, and brittle hair, cutaneous syndactyly affecting toes and/or digits, dysplastic nails, hyperkeratosis observable at the soles and at the skin folds of the hands, broad nasal base with pseudo-clefts starting from the nostrils, and oral synechiae. Histopathology of the lesional skin from the plantar region of the proband shows epidermal hyperplasia with marked hyperkeratosis and focal parakeratosis, initial spongiosis, and lymphocytic perivascular dermal infiltrate. Hematoxylin-eosin staining. Scale bar 200 μm.

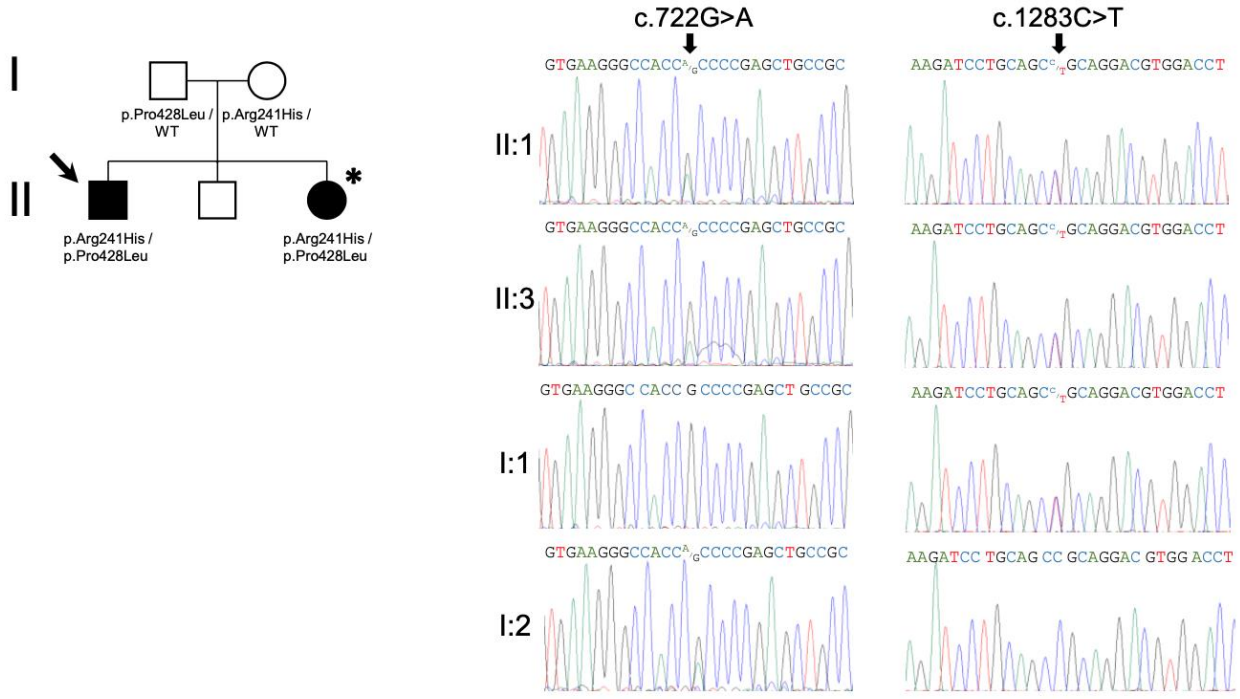

Figure 7. Pedigree of the family and electropherograms showing the segregation of p.Arg241His and p.Pro428Leu mutations. Arrow indicates the index patient (II:1) from whom the plantar skin biopsy (lesional) was obtained for histological, electron microscopy and immunofluorescence analysis. Asterisks indicate patient (II:3) from whom the primary keratinocyte cell line was created. On the right, Sanger sequencing chromatograms of exons 5 and 8 of *RIPK4* gene (NM_020639.2) showing the compound heterozygous variants (arrows)

2.1.2 Effect of mutations on RIPK4 activity

Modeling studies of newly identified *RIPK4* mutations showed that arginine 241 locates in the C-lobe of the kinase domain that contains the dimerization site and regulates the kinase activity. The interaction between Arg241 with other residues are crucial for protein stability and function of the protein. We hypothesized that the loss of this interaction, due to the p.Arg241His mutation disrupts both the tight interconnection network between the C-and N-lobe of the RIPK4 kinase domain and the propensity to form active homo-oligomers. Instead, p.Pro428Leu falls in the ankyrin repeat and lies in between two phosphodegron consensus sequences, recognized by ubiquitin E3 ligases. Mutations in proline residue may alter the protein local conformation and impair the interface regions that mediate interaction with regulatory kinases or the proteosomal complex. To ascertain the pathogenicity of the two novel mutations, wild-type and mutated recombinant RIPK4 were ectopically expressed in HEK293 cells. Expression of RIPK4 protein carrying the p.Arg241His variant resulted in completely loss of the hyper-phosphorylated pool, suggesting that this mutation inhibits the RIPK4 activity. Differently, the variant p.Pro428Leu variant only reduced the autophosphorylation activity (Figure 8).

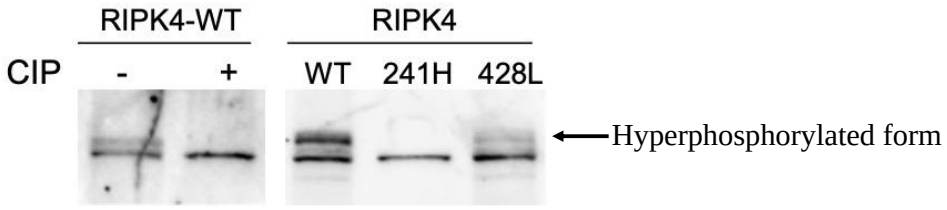

Figure 8. Novel identified variants interfere with RIPK4 activity.
In vitro phosphorylation analysis showing impaired auto-phosphorylation of RIPK4 mutant proteins. Myc-tagged wild-type (WT) and mutated (241H and 428L). RIPK4 recombinant proteins were transiently expressed in HEK293 and the presence of the hyperphosphorylated form was assessed by immunoblotting on total cell lysate using anti-Myc antibody. To confirm the hyperphosphorylated status of RIPK4-WT protein, the cell extract was treated with calf intestinal phosphatase (CIP) before immunoblotting (left panel). The data are representative of two independent experiments.

2.1.3 Functional effect of the RIPK4 missense mutations on IRF6 and p63

The effect of *RIPK4* mutations was investigated by evaluating activation and subsequent nuclear translocation of the RIPK4 phosphorylation target, IRF6, following their co-expression in HEK293 cells. By western blotting, IRF6 was mainly detect in the cytoplasm of the mock co-transfected cells, and an increased nuclear localization was observed in cells co-expressing wild-type RIPK4. However, IRF6 nuclear translocation was significantly reduced when it was co-expressed with the mutant RIPK4 proteins, either p.Arg241His or p.Pro428LeuFIG. These results indicate that the novel identified RIPK4 mutations lead to functionally defective proteins. In particular, the p.Arg241His abrogates the kinase function, while the p.Pro428Leu, even though still able to preserve RIPK4 kinase activity, affects its ability to activate IRF6 and partially prevents IRF6 nuclear translocation (Figure 9a). In addition, while no significant differences were observed in *TP63* expression at transcriptional level, accumulation of p63 protein was revealed by western blotting in *in vitro* patient differentiating keratinocytes, likely imputed to the reduced IRF6 activity (Figure 9b)

Consistent with the concept that p63 expression is principally restricted to cells with high proliferative potential and is absent from the cells that are undergoing terminal differentiation[46], we found high level of p63 protein and reduced expression of ectodermal differentiation marker (data not shown), suggesting a defective terminal differentiation process in patients' cells. Moreover, a strong reduction of abortive cell colonies was observed, compatible with a reduced number of terminally differentiated cells and augmented clonogenic potential, as demonstrated by the Colony Forming Efficiency assay (Figure 9c). In conclusion, RIPK4 defective function in patient keratinocytes affects proliferation/differentiation pathways causing a dysfunctional p63/IRF6 regulatory loop.

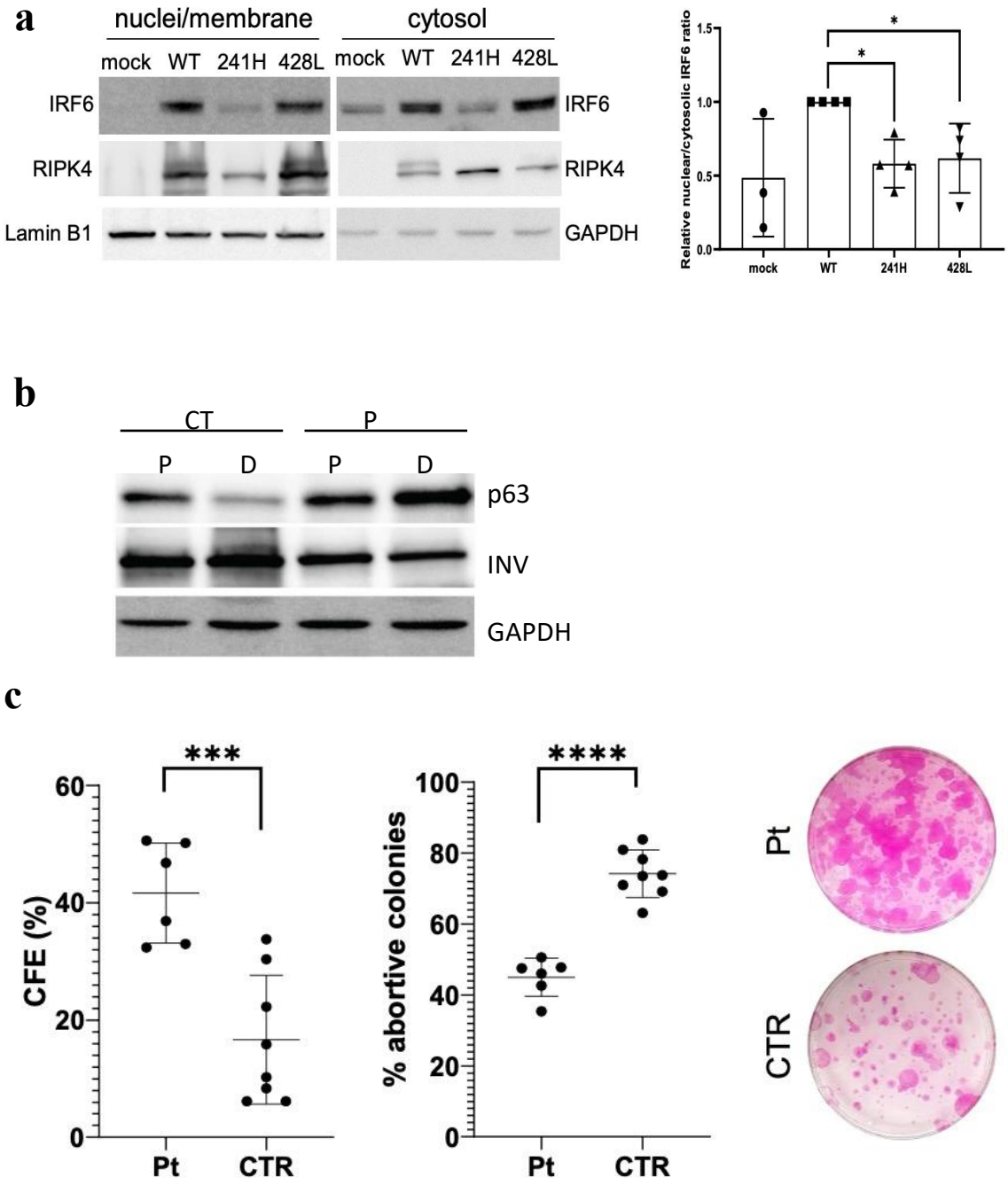

Figure 9. Novel identified variants interfere with RIPK4 activity.

a) *In vitro* IRF6 activation assay showing impaired activity of mutant RIPK4 proteins. HA-tagged IRF6 protein was transiently co-expressed with Myc-tagged WT or mutated (241H and 428L) RIPK4 proteins in HEK293. Thirty hours after transfection, protein fractions enriched for nuclear or soluble cytosolic components (nuclei and cytosol, respectively) were separated and analyzed by western blotting using anti-HA antibody to evaluate the IRF6 subcellular distribution. Anti- Myc antibody was used to confirm recombinant RIPK4 expression, anti-GAPDH and anti-Lamin B1 antibodies were used as cytosolic and nuclear fractions loading controls, respectively. On the right, graphical representation of the relative ratio between nuclear (active) and cytosolic (inactive) IRF6, calculated on 4 biological replicates, is shown. *p*-values were calculated using two-tailed paired *t*-test. *p<0.05.

b) Altered expression of keratinocyte differentiation markers in patient cells. Total protein extract from patient (Pt) and control (CTR) primary keratinocytes grown in proliferative (P, low calcium) or differentiating (D, 1.2 mM $CaCl_2$ for 72 hours) conditions were analyzed by immunoblotting with the indicated antibodies. Protein loading was normalized by GAPDH protein levels. A representative experiment out of 3 biological replicates is shown.
c) Clonogenic assay showing increased proliferative potential in RIPK4 defective keratinocytes. Colony forming efficiency (C.F.E.) and percentage of abortive colonies of patient II:3 primary keratinocytes as compared to the average values obtained using cells derived from two different control individuals matched by sex, age and passage numbers. On the right, representative plate images of clonogenic assay.

2.1.4 RIPK4 regulates PVRL4 gene transcription trough IRF6 activation

Given the overlap of patient clinical features with other EDs, in particular with EDSS1 caused by PVRL4 (nectin-4) deficiency, nectin-4 expression, which is normally induced during keratinocyte differentiation, was analyzed. Almost total absence was observed in patient's plantar skin, while membrane staining was detected in all suprabasal keratinocytes of the control skin biopsy (Figure 10a). However, E-cadherin appropriately decorated the cell borders indicating that adherens junctions were assembled. Altered nectin4 expression was also confirmed *in vitro* differentiated keratinocyte from patient biopsy, at protein level (Figure 10b). To establish whether a direct functional relationship exists between RIPK4 and nectin-4, nectin-4 expression was analyzed in control and patient keratinocytes treated with phorbol 12-myristate 13-acetate (PMA), a potent PKC activator that induce keratinocyte differentiation through RIPK4. A significant increase in nectin4 level was observed in normal human keratinocytes treated with PMA, concurrent with IRF6 induction and TP63 inhibition. Interestingly, patient cells showed neither the TP63 reduction nor the nectin-4 and IRF6 induction, supporting the hypothesis that nectin-4 expression is under RIPK4 control (Figure 10c). To obtain further insights into the regulation of nectin-4 by RIPK4/IRF6 axis, nectin4 expression was analyzed in *IRF6*-depleted primary keratinocytes. While nectin4 expression increased following calcium induced differentiation in control keratinocytes, no induction was observed in cells silenced for *IRF6* (Figure 10d). Taken together, these data indicate that *PVRL4* is a direct transcriptional target of IRF6.

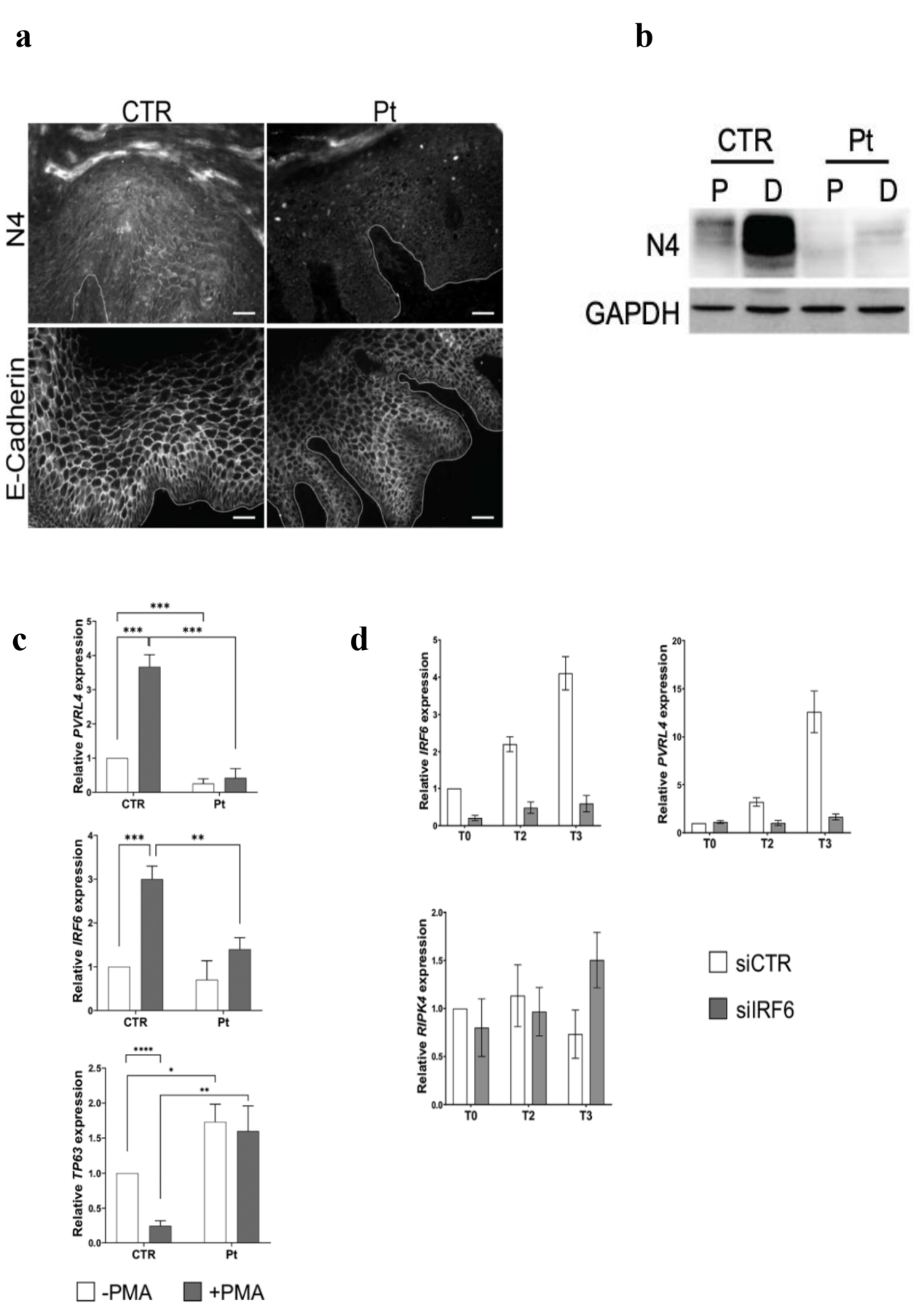
a
CTR
Pt
N4
E-Cadherin
b
CTR
Pt
P
D
P
D
N4
GAPDH
c
Relative PVRL4 expression
Relative IRF6 expression
Relative TP63 expression
CTR
Pt
-PMA
+PMA
d
Relative IRF6 expression
Relative PVRL4 expression
Relative RIPK4 expression
T0
T2
T3
siCTR
siIRF6

Figure 10. RIPK4 regulates transcriptional expression of *PVRL4* through IRF6 activation.
a) Analysis of expression and localization of adherens junction markers in patient skin showing loss of nectin-4 staining at cell–cell contact sites. Frozen sections of plantar skin obtained from an unaffected individual (CTR) and patient II:1 (Pt) were immunostained with anti-nectin-4 (N4) and anti-E-cadherin (E-Cad) antibodies. In the control sample, both N4 and E-Cad preferentially stains along cell–cell adhesion sites in all keratinocytes. In the patient skin, although a similar staining is observed with E-Cad, nectin-4 expression is strongly reduced, and its distribution altered. Scale bars 20 μm. b) Total protein extracts from patient (Pt) and control (CTR) primary keratinocytes grown in proliferative (low calcium, P) or differentiating (1.2 mM $CaCl_2$ for 72 hours, D) conditions were analyzed by immunoblotting with the indicated antibodies. Protein loading was normalized by GAPDH protein levels. A representative experiment out of 3 biological replicates is shown. c) Analysis of the effects of RIPK4 activation in human primary keratinocytes showing a functional relationship between RIPK4 and *PVRL4*, *IRF6* and *TP63* gene expression. Relative *PVRL4*, *IRF6* and *TP63* mRNA levels were evaluated by quantitative RT-PCR (RT-qPCR) in human primary keratinocytes obtained from an unaffected individual (CTR) and patient II:3 (Pt) after treatment with the PKC activator, phorbol 12-myristate 13-acetate (PMA). Levels were normalized to *GAPDH*. The relative expression values were determined via the ΔΔCt method. Average values ±SD of 3 independent experiments is shown. Asterisks, significant differences (**, $P<10^{-2}$; ***, $P<10^{-3}$; ****, $P<10^{-4}$, One-way ANOVA multiple comparisons test with Bonferroni's correction). d) Analysis of the effects of *IRF6* gene silencing in human keratinocytes showing loss of *PVRL4* expression. Relative *IRF6*, *PVRL4*, and *RIPK4* mRNA levels were evaluated by RT-qPCR in human primary keratinocytes transfected with *IRF6*-specific siRNA (siIRF6), and cultured *in vitro* in proliferating (low calcium, T0 = 24 h after transfection) or differentiating conditions (T2 and T3 = 48 and 72 h after 2 mm $CaCl_2$ supplementation, respectively). Transfection with a scramble sequence (siCTR) was used as control. Levels were normalized to *GAPDH*. The relative expression values were determined via the ΔΔCt method. Average values ±SD of 3 independent experiments is shown. Asterisks, significant differences (*, $P < 10^{-1}$; **, $P < 10^{-2}$; ****, $P < 10^{-4}$, One-way ANOVA multiple comparisons test with Bonferroni's correction).

2.1.5 Functional effects of the RIPK4 missense mutations on cell-cell adhesion in patient keratinocytes.

Histological observation of lesional patient plantar skin by hematoxylin-eosin staining showed epidermal hyperplasia, spongiosis and superficial dermal lymphocytic infiltrate (Figure 11a). Dilated intracellular spaces, cell-cell adhesion interruptions and loosening of cell-cell cohesion, were features observed in *in vitro* cultured patient keratinocyte colonies (data not show). None of these features were previously reported in EDSS1 specimens suggesting that additional adhesion complexes could be affected by mutated RIPK4. On the contrary, some phenotypic features, such as the thickening of the plantar skin, dystrophic nails, altered hair follicle development/alopecia, were shared with a disorder caused by biallelic mutations in *plakophilin-1*(*PKP1*), a crucial protein in maintaining desmosomal integrity. Thus, we decided to investigate PKP1's expression level by immunofluorescent analysis, in both patients and control palmar skin (Figure 11b). A remarkably reduction of PKP1 was observed, as also confirmed by transcript and protein analyses in *in vitro* cultured keratinocytes from patient (Figure 11c). To have more data about the stability of desmosomal plaque in the patients, we decided to investigate at least another two desmosomal adhesion molecules, desmoglein (DSG1) and desmoplakin (DSP). So, we carried out an immunofluorescence analysis, which showed a more diffuse DSG1 staining in the patient lesional skin, compatible with the widening of intracellular spaces between keratinocyte (Figure 11b). Regarding DSP, we observed a more diffuse cytosolic staining at cell-cell junction (Figure 11b). In addition, in collaboration with the Center of Microscopy at the University of L'Aquila, we investigated the desmosome structure in our patient skin and demonstrated an increase of the medium interspace, and a reduction of keratin filaments crossing the desmosomes, suggesting an impaired cell-cell adhesion (Figure 11d). In conclusion, mutations in *RIPK4* result in structural perturbation of desmosomes, likely consequent to altered PKP1 expression.

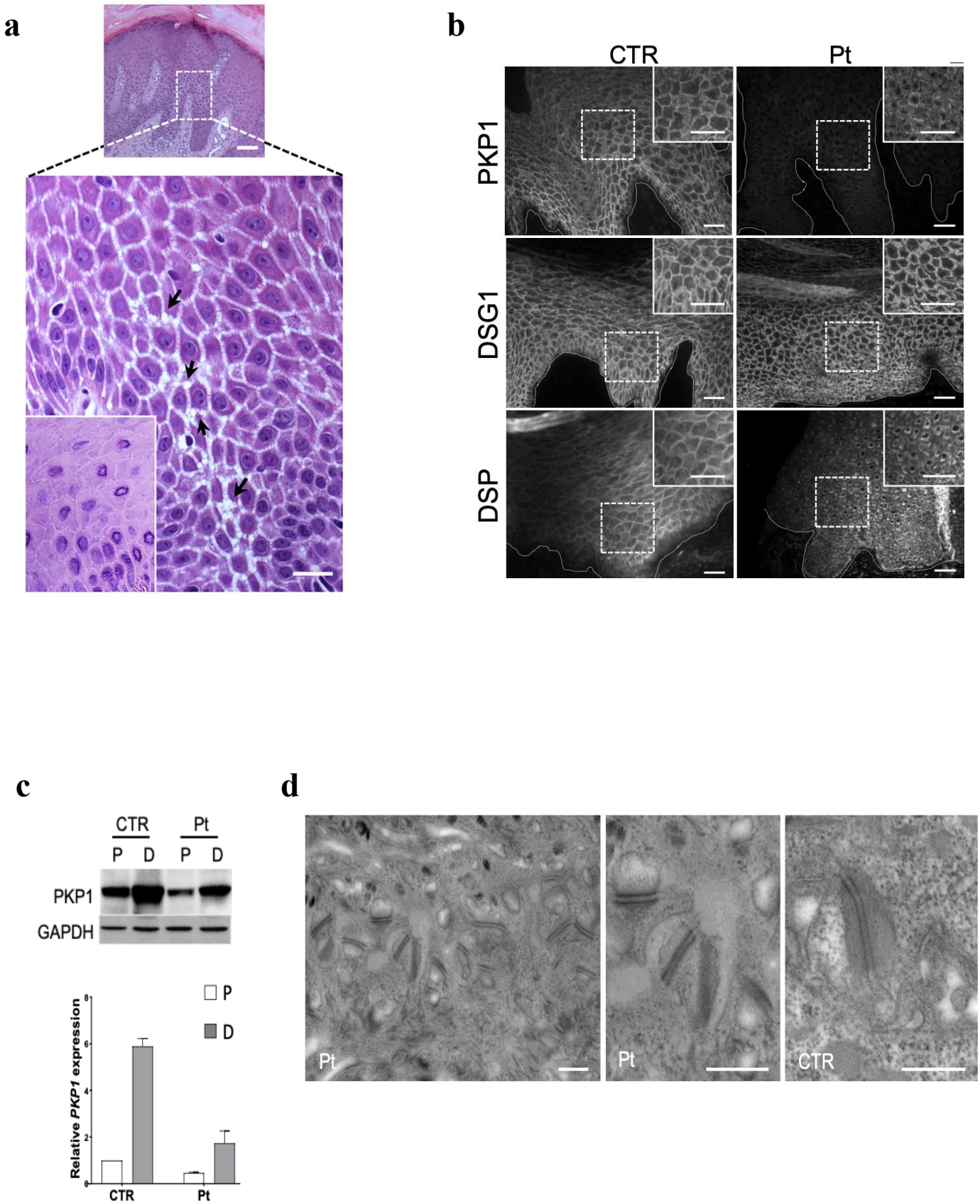
a
b
CTR
Pt
PKP1
DSG1
DSP
c
CTR
Pt
P
D
P
D
PKP1
GAPDH
P
D
Relative PKP1 expression
CTR
Pt
d
Pt
Pt
CTR

Figure 11. Desmosomal defects in *RIPK4* defective patients.

a) Histological analysis of patient lesional skin, showing focal loss of cell cohesion and widening of intercellular spaces in the spinous layer. Higher magnification of the hematoxylin–eosin staining of patient II:1 plantar skin is shown. Spinous layer keratinocytes have lost their typical polygonal shape and several micro-detachments are evident between the rounded cells (arrows). Insert: hematoxylin–eosin staining of control plantar skin. Scale bar 20 μm (scale bar of the miniature 100 μm).

b) Analysis of expression and localization of desmosomal markers showing altered expression and distribution in patient epidermis. Frozen sections of plantar skin obtained from an unaffected individual (CTR) and patient II:1 (Pt) were immunostained with anti-plakiphilin-1(PKP1), anti-desmoglein-1 (DSG1), and anti-desmoplakin (DSP) antibodies. In the control sample, both PKP1, DSG1, and DSP preferentially stains along cell-cell adhesion sites in all keratinocytes. In the patient skin, PKP1 staining intensity is strongly reduced and almost absent at cell-cell contact sites; DSG1 staining at cell membrane is outstretched suggestive of widening of intercellular spaces between keratinocytes; DSP is aberrantly distributed and shows a diffuse staining in the cytoplasm. Scale bars 20 μm.

c) Analysis of PKP1 expression in primary keratinocytes showing reduced protein and mRNA levels in patient cells. Total protein extracts from patient (Pt) and control (CTR) primary keratinocytes grown in proliferative (low calcium, P) or differentiating (1.2 mM $CaCl_2$ for 72 hours, D) conditions were analyzed by immunoblotting with the indicated antibodies. Protein loading was normalized by GAPDH protein levels. A representative experiment out of 3 biological replicates is shown.

Analysis of *PKP1* expression in primary keratinocytes showing a strong reduction of the transcript in patient cells. Relative *PKP1* mRNA expression, as determined by RT-qPCR using cDNA obtained from primary keratinocytes of unaffected individual (CTR) and patient II:3 (Pt) cultured in in proliferative (P, low calcium medium) or differentiating (D, 1.2 mM $CaCl_2$ for 72 hours) conditions. The relative expression values were determined via the ΔΔCt method. Average values ± SD of 2 independent experiments is shown.

d) Transmission electron microscopy micrographs showing numerous wide intercellular spaces and low electron-density patches, resembling vacuoles, in the proximity of cell borders in patient skin (Pt). A representative micrograph of control patient II:1 skin (CTR) showing well-preserved ultrastructure is shown in the panel on the right. Scale bars 0.5 μm.

2.2 Discussion

In our work, we showed how the synergy among phenotype analysis, NGS strategy and functional study lead to define a more detailed genotype-phenotype correlation and to establish a mutual relationship and a molecular hierarchical among genes whose mutations result in a similar phenotype. In the context of EDs we studied two siblings with cutaneous syndactyly, associated to hair defects, alopecia, nail dysplasia and hyperkeratosis who were seeking for a diagnosis. Considering that a similar phenotype was shown in patients with EDSS1, caused by biallelic mutations in *PVRL4* encoding for the cell adhesion molecule nectin4 and representing a major constituent (together with E-cadherin) of adherents junctions[47], we decided to analyze potential mutations in this locus. Interestingly, *PVRL4* gene was not mutated, whereas we identified novel *RIPK4* biallelic variants. These results expand the clinical spectrum seen in *RIPK4*-pathies. So far, homozygous missense mutations located in the kinase domain or truncating variants result in early lethality (BPS phenotype), while missense variants in the ankyrin repeats domain were found in survivors (featuring cutaneous webbing across one or more major joints, cleft lip and/or palate). For the first time, we reported a compound heterozygosity, i.e. p.Arg241His and p.Pro428Leu variants located in the kinase domain and in the second ankyrin repeats of RIPK4, respectively, which give rise to an intermediate phenotype. In fact, both our siblings displayed cutaneous syndactyly of hands and feet. To date such phenotypic features were not described in patients with CHAND syndrome[39-40-48](a less severe disorder), while were present in BPS (more severe form). As recently reported on the NCBI archive ClinVar, homozygosity mutations p.Arg241His are associated with BPS phenotype. Considering these data, we can speculate that the combination of these two mutations are less deleterious probably because the p.Pro428Leu and p.Arg241His mutation combination allows for partial functions of RIPK4. In addition, since the phenotype here described overlaps with EDSS1, IRF6- and TP63-pathies and with patients carrying biallelic mutation in *PKP*-1, we postulated the existence of a regulatory mechanism between P63, RIPK4, IRF6, PKP-1 and PVRL4.[35-49] Indeed, our results extend the description of the molecular framework involved in ectodermal morphogenesis and homeostasis, that includes intricate feedback regulatory loops between transcription factors and protein kinases, and downstream functional regulation of cell adhesion structures. Our data identify the p63-dependent expression of both IRF6 and RIPK4 as the first mandatory step of the ectodermal-specific differentiation program. Then IRF6 activation by RIPK4-dependent phosphorylation is necessary for the degradation of p63, inhibits cell proliferation and activate transcription of epithelial differentiation markers, including *PVRL4*/nectin4. In parallel, RIPK4 regulates cell adhesion function by phosphorylation of cell adhesion molecules (i.e. the desmosomal protein PKP1). p63, on the other side, controls also the expression of several other molecules that take part to the cell-adhesion

program (Figure 12). So, this work led to add nectin4 and RIPK4 as new players in the p63 and IRF6 network, clarifying the processes regulating the balance between proliferation and differentiation. Moreover, these results extend the features associated to mild phenotype caused by RIPK4 mutation, including syndactyly in this condition.

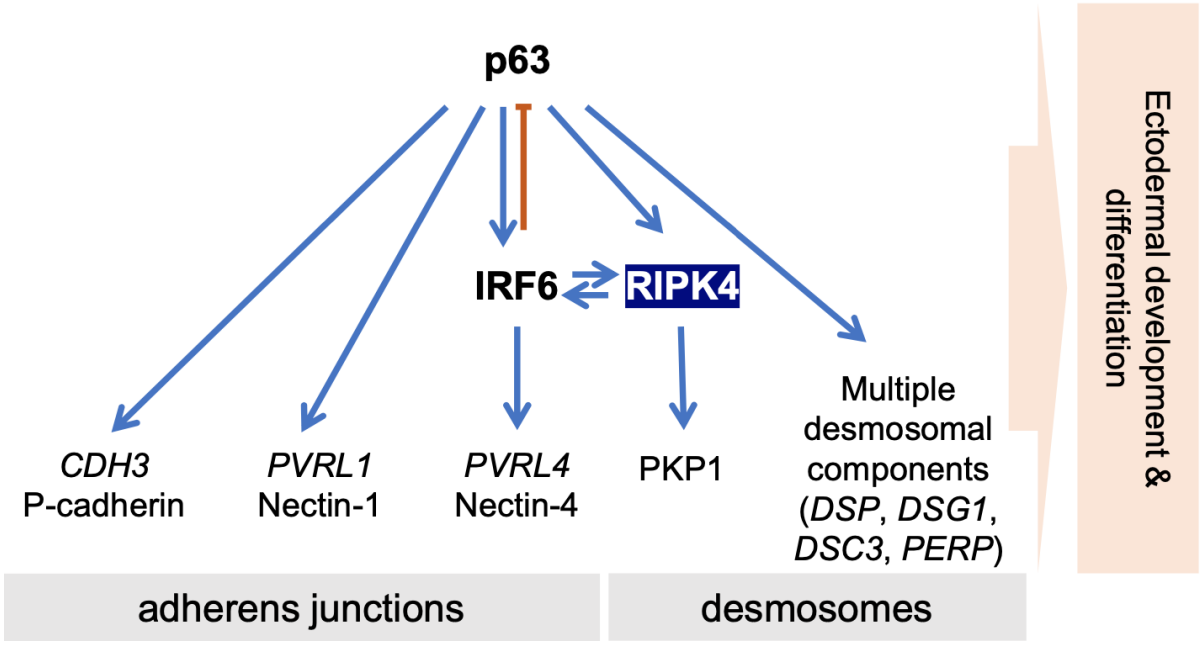

Figure 12. Schematic representation of the link between RIPK4, p63, IRF6, and adhesion molecules.
RIPK4 is part of the p63-IRF6 regulatory loop that control epidermal development and proliferation/differentiation balance in skin homeostasis through a multistep regulation of the cell-cell adhesion function. RIPK4, under the balanced control of p63 and IRF6 transcription factors, phosphorylates and activates IRF6 protein, which in turn induces p63 degradation, reducing proliferative potential of epithelial cells and inducing keratinocytes differentiation. Both p63, IRF6 and RIPK4 regulate expression or function (by phosphorylation) of cell adhesion molecules mainly involved in adherens junction and desmosome assembly.

2.3 Material and Methods

2.3.1 Genetic Investigation

Blood genomic DNA was submitted to clinical exome sequencing analysis (Trusight One panel, Illumina, San Diego, CA, USA), using a NextSeq 500 platform, with 30x average sequencing coverage. Read files were obtained from the Illumina platform through the manufacturer's proprietary software (Illumina Variant Studio Software v3.0). Variant annotation and prioritization have been performed using the eVai platform (enGenome, Pavia, Italy). In particular, we selected for variants predicted to alter protein products (exonic and splicing, non-synonymous SNVs) presenting a minor allele frequency (MAF) < 0.01 in GnomAD, ExAC, 1000GP, and ESP databases. Next, we excluded polymorphic genes and genes harboring a single heterozygous variant. Finally, we focused on the homozygous and compound heterozygous variants shared by both the affected siblings (n=37) (Supplementary Tables 1 and 2). Among 9 genes harboring these 37 variants, the only disease-causative gene implicated in a condition compatible with our patient phenotype was *RIPK4*, in which two distinct missense changes were observed: c.722G>A (p.Arg241His) in exon 5 and c.1283C>T (p.Pro428Leu) in exon 8. SIFT, PolyPhen and Provean predictors were interrogated to score the pathogenicity of missense variants (Supplementary table 3). Both variants were validated and segregated in family members by Sanger sequencing (Supplementary figure 1A). Mutation effects on splicing were experimentally tested by reverse transcriptase (RT)-PCR analysis of the total RNA purified from cultured keratinocytes of patient II:3 using primers (F)-catggatggcctgtttggca (exon 3) and (R)-ttggcattgttgagcagcag (exon 8) that amplify across mutation sites. The identity of the amplified cDNA product was determined by Sanger sequencing.

2.3.2 Transient transfections, protein phosphatase treatment, and in vitro IRF6 activation assay

HEK293 cells grown to 70% confluence were transiently transfected with pCMV-Myc-RIPK4-wt, pCMV-Myc-RIPK4-241H, pCMV-Myc-RIPK4-428L or an empty vector, using Lipofectamine 2000 reagent (Invitrogen) and following manufacturer's instruction. Thirty hours after transfection cells were harvested in Laemmly buffer and analyzed by western blotting. Cells transfected with pCMV-Myc-RIPK4-wt were also lysed NP40 buffer (50 mM Tris pH 8.0, 150 mM NaCl, 1% NP40) supplemented with Complete protease inhibitor cocktail (Sigma-Aldrich). Lysates were cleared by centrifugation and treated with CIP (New England Biolabs), 100 units of enzyme in 50 µl. Treated and untreated samples were incubated at 30 °C for 30 min and analyzed by western blotting. For the IRF6 activation assay, pCDNA-HA-IRF6 was co-transfected with pCMV-Myc-RIPK4-wt, pCMV-

Myc-RIPK4-241H, pCMV-Myc-RIPK4-428L or an empty vector. Thirty hours after transfection cells were either fixed in 4% paraformaldehyde and processed for immunofluorescence or recovered by scraping in ice cold fractionation buffer (250 mM Sucrose, 20 mM Hepes pH 7.4, 10 mM KCl, 1.5 mM MgCl2, 1mM EDTA, 1mM EGTA) supplemented with Complete protease inhibitor cocktail. Cells suspension was then passed through a 25-gauge needle syringe 10 times (or until all cells were lysed) and left on ice for 20 minutes. The fraction N, enriched for the nuclear components, was recovered by centrifugation at 720 g (3,000 rpm) for 5 minutes at 4°C, while supernatants, containing cytoplasm, cytoskeleton, membrane and mitochondria were collected as cytosolic fraction (Cy). Pellets were resuspended in 0.5 volumes of 2x Laemmli sample buffer. Equal volume of N and Cy fractions in Laemmli buffer were boiled 10 minutes at 95°C, separated on 10% SDS-PAGE, and analyzed by western blotting. To evaluate the RIPK4 activity, nuclear localization of IRF6 protein was assessed either by immunofluorescence (number of cells with nuclear IRF6 staining/total IRF6 positive cells ratio) or densitometric analysis of western blotting bands (nuclear IRF6/cytosolic IRF6 ratio).

2.3.3 Western blotting analysis

Protein samples in Laemmly buffer were run under reducing conditions, using 10% or 12% SDS-polyacrylamide gels, transferred on nitrocellulose membrane and immunoblotted with indicated primary antibodies. Specific signals were revealed using HRP-conjugated secondary antibodies and detected with Amersham ECL Prime (GE Healthcare Life Sciences, Little Chalfont, UK). by using Bio-Rad ChemiDoc Imaging System. Signals were analyzed and quantified by using ImageLab software (Bio-Rad, Hercules, CA, USA).

2.3.4 Clonogenic assay

Primary keratinocyte from patient II:3 and two control individuals matched for age, sex and number of passages were seeded on irradiated 3T3-J2 feeder layer (10 3 cells/100 mm dish plate) and incubated in keratinocyte medium for two weeks. Media was replaced every 3 days. Colonies were then stained with 0.005% crystal violet dissolved in 20% ethanol solution. Colonies were counted manually. Colony forming efficiency (C.F.E.) correspond to the number of colonies on the total 8 amount of plated cells (Number of colonies/Number of cells seeded) x100. Paraclones (abortive colonies) were identified based on their peculiar morphology (very small, punctiform colonies, formed by a small number of senescent and differentiated cells), and percentage of abortive colonies was calculated as number of abortive colonies on the total number of colonies.

2.3.5 IRF6 silincing

Primary keratinocytes from healthy individuals were transfected with stealth siRNA duplexes targeting human *IRF6* (HSS105511–HSS105512–HSS105513) or siRNA negative control duplexes (Invitrogen) using Lipofectamine RNAi Max reagent (Invitrogen) according to the manufacturer's instructions in KGM medium. Twenty-four hours after transfection (*T*=0) the cells were induced to differentiate by supplementation with 1.2 mm Ca++for48(*T*=2)or72(*T*=3)h. At each time point, cells were recovered and analyzed by western blotting and RT- qPCR. *IRF6* silencing efficiency was verified at mRNA and protein levels.

2.3.6 RNA isolation and analysis

Total RNA was isolated from differentiated primary keratinocytes using TriZol® (Invitrogen) according to the manufacturer's guidelines. RNA was reverse transcribed into cDNA using Super Script III (Invitrogen) and analyzed by real-time RT-qPCR using either TaqMan gene expression assays (*Applied Biosystems,* Carlsbad CA, *USA) or Sybrgreen Mastermix (Applied Biosystems)*. Primer sequences are listed in Supplementary Table 4. The relative expression values were determined via the ΔΔCt method. Experiments were run in triplicate.

2.3.7 Light microscopy and transmission electron microscopy

Tissue biopsies collected from the plantar skin of patient II:1 and a control individual were washed in phosphate- buffered saline (PBS) and immediately fixed in 2.5% glutaraldehyde (Agar Scientific, Cambridge Road Stansted Essex, UK) in PBS. To allow a correct penetration of the fixative, all samples were cut with a razor blade to a size of ∼2 × 2 mm and stored with fresh glutaraldehyde (2.5%/PBS) at 4°C for at least 48 days. Samples were, then, rinsed in fresh PBS (3 changes, 30 min each in stirring), post-fixed with 1% osmium tetroxide (OsO4) (Agar Scientific, Stansted, UK) in PBS for 1 h and rinsed again in PBS (1 × 30'). After that, biopsies were dehydrated in the ascending series of ethanol, with the following subsequent passages: EtOH 30%, EtOH 50%, EtOH 70% (1 × 10'), EtOH 95% (2 × 10') and EtOH 100% (4 × 15'). Following the immersion in propylene oxide (PO) (2 × 20') for solvent substitution, samples were infiltrated in PO/Epoxy resin (1:1) overnight, embedded in the epoxy resin EMbed-812 (Electron Microscopy Sciences, 1560 Industry Road, Hatfield, PA, USA) for 48 h at 60°C and sectioned using a Reichert-Jung Ultracut E ultrami- crotome. Semi-thin sections (1 mm thick) were stained with Toluidine Blue, examined using light microscopy (LM; Zeiss Axioskop) and photographed using a digital camera (Leica DFC230). Ultrathin sections (60–80 nm) were cut with a diamond knife, mounted on copper grids and contrasted with Uranyless

and lead citrate (SIC, Rome, Italy). They were examined and photographed using Zeiss EM10 and Philips TEM CM100 Electron Microscopes operating at 80 kV.

Chapter 3: Phe142Leu in the GJB2 gene causes Keratoderma-Deafness-Mucocutaneous Syndrome

3. Introduction

In this work, I focused on hereditary hearing loss caused by mutations in *GJB2* gene codifying for the connexin 26 (Cx26), a component of the Gap Junction. Gap Junctions are involved in cellular communication important for the maintenance of tissue/organ homeostasis. Using this communication, cells can perceive differences in environmental conditions and respond accordingly. This concept could involve either sending a signal to neighboring cells to generate a coordinated response or isolating groups of cells from the rest of the community to maintain tissue integrity. Gap junctional channels link the cytoplasm of two cells, and provide a means for the exchange of ions (K^+ and Ca^{2+}), second messengers (cAMP, cGMP, and inositol 1,4,5-triphosphate (IP_3)), and small metabolites (glucose), allowing electrical and biochemical coupling between cells.[50-51]

Gap junction channels are formed by connexin protein subunits, six of which combine to produce a hemichannel.[52] Two hemichannels from the plasma membranes of adjacent cells align in the extracellular space to form a complete gap junctional channel.[53] In addition, connexin hemichannels can be functional in non-junctional membranes, allowing the exchange of solutes with the extracellular space.[54-55] There are more than 20 connexin genes and nearly all cells in the body express at least one type of these genes at some point during development and in adult life. For instance, Cx26 is highly expressed in cochlea, liver, skin, and placenta, while Cx46 and Cx50 are exclusively found in the eye. Moreover, connexins show overlapping expression patterns where an individual cell expresses more than one type of isoform. Cx26, Cx30, Cx30.3, Cx31, Cx43, and others, for example, are found in keratinocytes[56], to note that Cx26 is only present in the palmoplantar epidermis layer.[57] Gap junction channels may be assembled from the same connexin, or a combination of different connexins, depending on the cell type. Each connexin protein has four transmembrane domains (TM1 – TM4), connected by two extracellular loops (EC1 and EC2) and a cytoplasmic loop (CL).[58] The N- and C-termini of the protein extend into the cytoplasm of the cell.[58] Two organs where connexins and gap junctions are necessary for normal function are the skin and the inner ear.[58] Mutations in connexin genes have been linked to human hereditary diseases affecting both the epidermis and cochlea.[59] Of note, homozygosity mutations in *GJB2* are almost exclusively associated with hearing impairment (non-syndromic hearing loss) while heterozygous mutations have a pleiotropic effect (syndromic hearing loss) and cause a spectrum of different, partly overlapping conditions known as Bart-Pumphrey syndrome (BPS; OMIM #149200), Hystrix-like ichthyosis with deafness (HID; OMIM

#602540), Keratitis-ichthyosis-deafness syndrome (KID; OMIM #148210), Keratoderma palmoplantar with deafness (PPK; OMIM #148350) and Vohwinkel syndrome (VS; OMIM #124500)[59]. The aim of this work was to compare the phenotype of a patient carrying a heterozygous variant in *GJB2* and 4 subjects from 3 families found in the literature who carried the same aminoacidic substitution.

3.1 Results

3.1.1 Patient description

A 41-year-old woman was examined for chronic recurrent dermatitis mainly characterized by erythema, papules and plaques that healed leaving cicatricial sequelae, associated with bilateral high frequency sensorineural hearing loss. Three days after her birth, she had been hospitalized for diffuse severe erythematous lesions over the face (cheeks), lower limbs, inguinal and intergluteal skinfolds associated with severe erythema of the oral mucosa (especially the hard palate) and perianal region. She was discharged with a diagnosis of maculopapular exanthema. Recurrent episodes of intermittent angular cheilitis were registered during childhood and adolescence together with intermittent eruptions of scaly erythematous plaques, the most affected areas being neck, trunk, pubis and the inguinal and axillary folds. Cyclosporine therapy was started after a diagnosis of psoriasis with dramatic worsening of the disease. Premature loss of permanent teeth was recorded at 25 years. At the age of 33 years, erythematous, scaly and edematous lesions with clearly defined borders were noticed in the pubic area and inguinal folds, while erythematous papules and pustules involved the trunk. A skin biopsy of a plaque in the area of the mons pubis revealed epidermal hyperplasia, hyperkeratosis with focal parakeratosis and a dermal infiltrate rich in lymphocytes and neutrophils, with numerous spores, hyphae and pseudo-hyphae in the horny layer. *Candida albicans* was cultured from this specimen and antimycotic therapy was started with limited improvement of lesions attributable to candidiasis. Laboratory analyses revealed lymphocytopenia with decreased T-lymphocytes CD4, CD8 and natural killer cells. At last examination, aged 41 years, she showed papulopustular acne lesions on the face (Figure 13a, b), erythematous papules on the trunk (Figure 13c, d), focal plantar keratoderma (Figure 14e) that contiguously extended to the Achille tendon region (Figure 13f) and minimal hyperkeratosis on the palmar aspect of the first interdigital spaces (Figure 13g, h). Hair, nails and sweating were not affected.

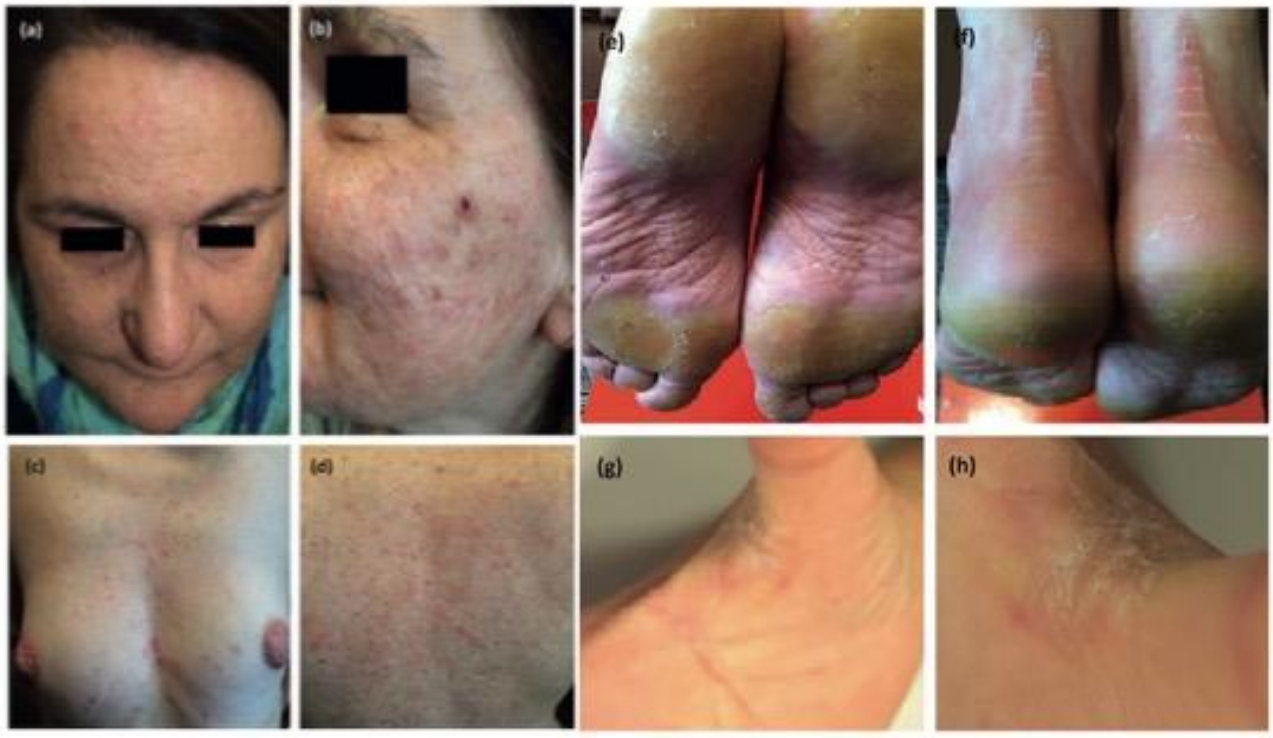

Figure 13. Patient's characteristics. (a, b) Papulopustular acne lesions on the face. (c, d) Erythematous papules on the trunk. (e, f) Focal plantar keratoderma contiguously extending to the tendon regions (transgrediens). (g, h) Minimal hyperkeratosis of the first interdigital spaces.

3.1.2 Genetic investigations

Due to the association of keratoderma and hearing loss, Sanger sequencing analysis of the GJB2 gene was started in the proband and revealed a single heterozygous nucleotide substitution c.426C>A, absent in her parents supporting its de novo origin. This variant (rs397516877 in dbSNP) was absent in gnomAD database and caused the p.Phe142Leu change scored as "pathogenic" by prediction systems such as MutationTaster, PolyPhen2 and Mutation Assessor. The Sanger sequencing is shown in Figure 14.

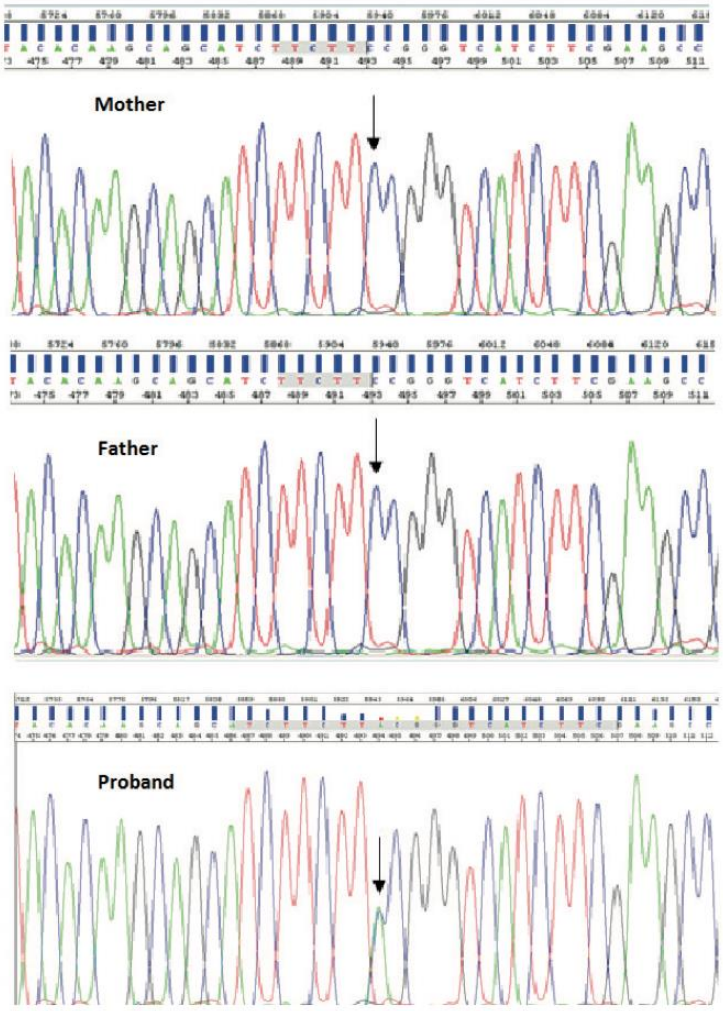

Figure 14: Identification of the GJB2 variant. Electropherograms of GJB2 exon 2 sequence encompassing the c.426C> A variant, present at the heterozygote state in the proband and absent in her parents (arrows).

3.1.3 Comparation among features of patients with hearing loss and unusual mucocutaneous findings due to Phe142Leu in GJB2

As reported in the literature, 3 families with 4 patients harboring this missense change existed: two families had a c.424T>C nucleotide substitution and one the same c.426C>A variant identified in our patient.[60-61] At clinical comparison, phenotypic overlap was evident especially at neonatal age. Indeed, most of the patients are described as neonates or infants, when the phenotype is particularly manifested with unusual cutaneous and mucous manifestations resembling mucocutaneous candidiasis being constantly seen. Dermatologic lesions were variably described as psoriasiform dermatitis, erythematous macules, patches and plaques. Angular cheilitis was recorded in all patients. Some individuals had inflammation of oesophageal mucosa. Squamous cell carcinoma of the hard palate was registered once. Susceptibility to infections was common although laboratory investigations, when conducted, excluded immune deficiencies. Interestingly, in our patient we recorded lymphocytopenia with decreased CD4, CD8 and natural killer cells, which can at least in part contribute to such susceptibility. Despite a number of common features observed among p.Phe142Leu mutated patients, some differences exist. In fact, palmoplantar keratoderma and papulopustular acne have never been reported before, probably due to the very early age of the cases previously described; interestingly, skin and mucosa biopsies of two other p.Phe142Leu patients showed hyperkeratosis[60-61], while severe nodulo-cystic acne was described in KID.[62]

Table 2. Features of patients with hearing loss and unusual mucocutaneous findings due to Phe142Leu in *GJB2*

Characteristics	Patients				
	Family 1, Patient II;1	Family 2, Patient II;1	Family 3, Patient II;1	Family 3, Patient I;2	Family 4, Patient II;1
Reference	Brown et al., 2003 (6)	Rednam et al., 2011 (7)	Ibanez et al., 2013 (8)	Ibanez et al., 2013 (8)	Present case
GJB2 gene (NM_004004.5)	c.424T>C	c.424T>C	c.426C>A	c.426C>A	c.426C>A
Connexin 26 (NP_00399.2)	p.(Phe142Leu)	p.(Phe142Leu)	p. (Phe142Leu)	p.(Phe142Leu)	p.(Phe142Leu)
Inheritance	Het; de novo	Het; de novo	Het; mat	Het; NA	Het; *de novo*
Age at description, years	2	6	Birth	23	41
Sex	F	F	F	F	F
Sensorineural hearing loss	+	+	+	+	+
Cutaneous involvement					
Lesions at birth	–	–	+	–	+
Psoriasiform dermatitis	+	+	–	–	+
Acne with cicatricial sequelae	–	–	–	–	+ (adulthood)
Palmoplantar keratoderma	–	–	–	–	+
Calcinosis cutis	+ (both heels)	–	–	–	–
Erythematous lesions	+ (periorificial, face, trunk upper extremities and diaper areas)	–	+ (intertriginous areas, scalp)	+ (head, neck, trunk)	+ (face, trunk, limbs, periorificial)
Whitish lesions	–	–	+ (papules on the scalp and upper limbs)	+ (external auditory canal, labial commissures and subauricular areas)	–
Skin histopathology					
Hyperkeratosis	+ (orthokeratotic)	NA	+ (epidermal and follicular)	NA	+
Parakeratosis	+ (focal)	NA	+ (epidermal and follicular)	NA	+ (focal)
Acanthosis	+	NA	–	NA	–
Papillomatosis	+	NA	–	NA	–
Foci of acute and chronic inflammation	+ (superficial derma and epidermis)	NA	+ (perifollicular inflammatory infiltrate)	NA	+ (superficial derma and epidermis)
Adnexal involvement					
Alopecia	+	–	+	–	–
Nail dystrophy	–	–	+	–	–
Oropharyngeal involvement					
Multiple dental lamina cysts	+	–	–	–	–
Teeth anomalies	+ (focal enamel hypoplasia of primary teeth)	NA	NA	NA	+ (premature loss of permanent teeth)
Angular cheilitis	+	–	+	–	+
Gingivitis	+	+	–	–	–
Erythema, focal ulceration, adherent white plaques	+	–	–	–	+
Endoscopy of upper gastrointestinal tract					
Inflammation of oesophageal mucosa	+ (denuded and friable mucosa)	+ (esophagitis)	+ (parakeratosis)	+	–
Oesophageal stricture	+	–	–	+ (oesophagocoloplasty)	–
Tumoral lesions					
Squamous cell carcinoma	–	+ (hard palate)	–	–	–
Recurrent infections	+ (urinary tract infections, perirectal abscesses, otitis)	+ (perirectal abscesses)	+ (2episodes of sepsis)	–	+ (candidiasis)
Other	Iron deficiency anaemia, reactive thrombocytosis; mild delay in myelination	–	Double left excretory renal system; anaemia and transient neonatal hypocalcaemia; cyst of choroid plexus	–	Verrucous haemangioma; lymphocytopaenia with decreased CD4, CD8 and natural killer cells

+ Present; – absent; het: heterozygous; mat: maternal; NA: not available; F: female; pat: paternal. In the family by Ibanex et al. (8) the father, homozygote c.35delG in *GJB2*, transmitted this additional mutation to his daughter.

3.2 Discussion

Here, we report a 41-year-old patient carrying a heterozygote mutation "p.Phe142Leu" in the *GJB2* gene, displaying the association between distinct mucocutaneous phenotype with hearing loss. A significant phenotypic overlap was evident among our patient and four patients from three additional families. This study highlights how different mutations in a same gene (*GJB2* in this case) can result in distinct phenotypes with subsequent extra degree of complexity to make a diagnosis. Previously studies showed that *GJB2* mutations result in non-syndromic or syndromic hearing loss dependent on the pattern of hereditary and the location of the mutations. Autosomal recessive mutations are associated with hearing loss without skin involvement (non-syndromic hearing loss) probably because of a simple loss of channel function altering only the cochlear intercellular communication[63-64], and suggesting that loss of connexin function is not detrimental for the development and function of the epidermis. On the other hand, autosomal dominant mutations showed an alteration or gain-of-function provoking skin disorders and ectodermal dysfunction (syndromic hearing loss), as well as deafness.[65-66-67-68] Moreover, regarding syndromic hearing loss, a correlation was emerged between different syndromes and specific domain mutations of Cx26. Of note, variants causative of KID syndrome map to CL, TM1 and EC1 domains of Cx26, involved in channel gating and regulation, and rarely to TM2 domain.[69] Variants underlying VS, BPS and PPK mostly map to EC1 and to transition zone between EC1 and TM2, with sporadic cases affecting EC2 and CL domains[70] (Figure 15).

Phe142 residue lies at the beginning of TM3 (residues 129–159) with its side chain protruding into the membrane bilayers and being about 30 Å distant from the pore shrinkage. Notably, closely located mutations such as Thr135Ala or Val153Ile, also with side-chains buried in the membrane bilayers and far from functional sites of the hemichannel, are associated to non-syndromic hearing loss. As the p.Phe142Leu, these changes preserve the hydrophobic features of TM3 and are not predicted to differently affect channel architecture and stability; accordingly, more subtle conformational alterations might explain the different phenotypic consequences. We speculate that distinct mutations in TM3 helix may differentially influence the conformation of CL domain, connecting TM2 and TM3 and altering the interactions with its substrates. In particular, Phe142 is in contact with Pro87, which belongs to TM2 and disrupts its H-bond array inducing a bent of this structural element. Consequently, a loosen interaction due to the p.Phe142Leu substitution may both alter the relative orientation of TM2-TM3 and, indirectly, the CL conformational states. Notably, this structural feature mediates the majority of protein-protein interactions of a connexin hemichannel, including those with kinases (fundamental to regulate its open-to-close transition) and with other proteins necessary for

anchoring to cytoskeleton.[71] In conclusion, this work helped to amply the clinical phenotype adding two features, i.e. palmoplantar keratoderma and papulopustular acne, which were never been reported in association with mutation in Phe142Leu in previous studies. In addition, we performed structural studies to investigate the impact of mutations affecting distinct domains on specific phenotypic features.

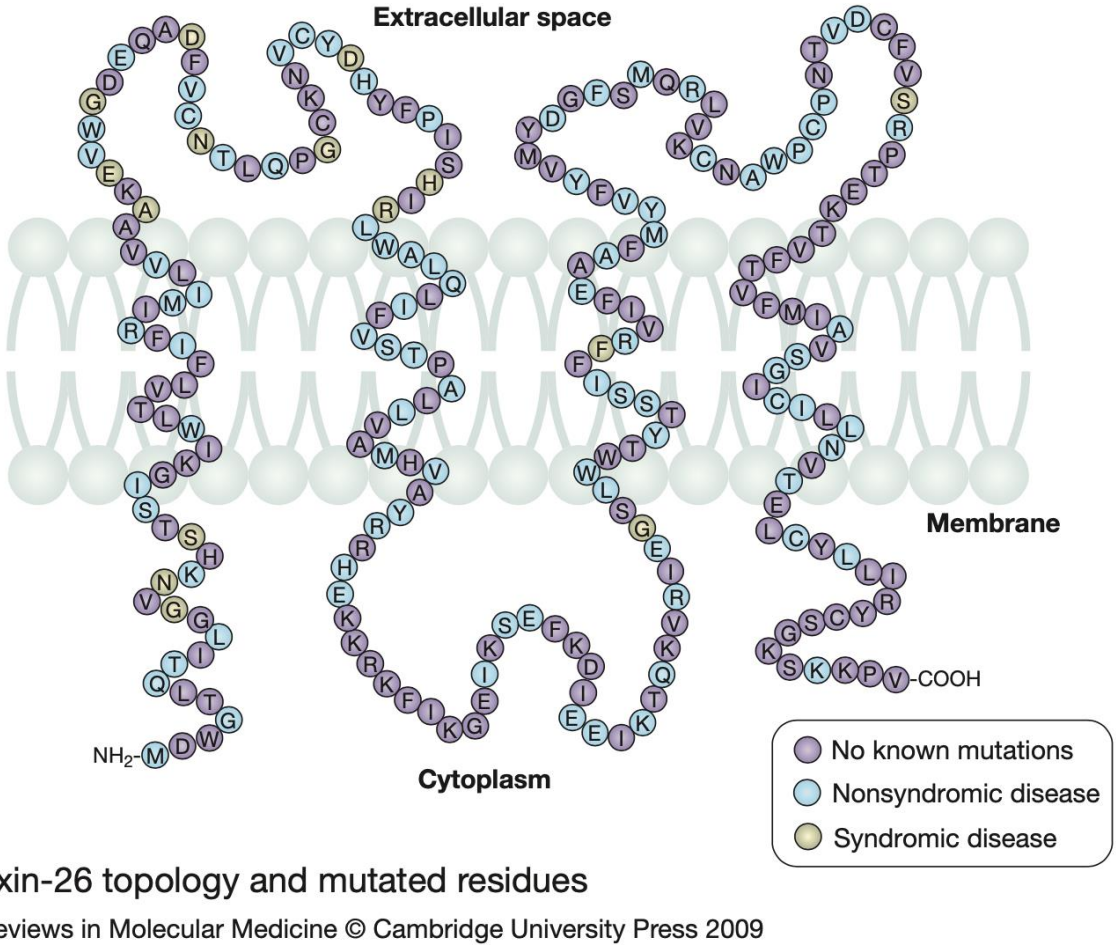

Figure 15: Connexin-26 topology and mutated residues. This illustration displays the location of amino acid residues in Cx26 relative to the membrane. Purple residues are not mutated. Blue amino acids are mutated residues found in non-syndromic deafness and can be seen throughout the protein. Brown residues represent amino acids mutated in syndromic deafness, which are generally found within the N-terminus and first extracellular loop.

3.3 Material and Methods

3.3.1 Sanger sequencing

Mutational screening of *GJB2* (NM_004004.6) was performed by PCR amplification of purified blood genomic DNA using primers encompassing the entire coding region of the gene (exon 2, 680 bp), followed by direct Sanger sequencing of the resulting PCR fragment. Primers used were (Fw) 5'-ccagagcaaaccgcccagag and (Rv) 5'-tcttaatctaacaactgggc.

Conclusion

In this thesis, we emphasized the importance of a multidisciplinary approach consisting of clinic, genetic and functional biology studies. These three fields are to be considered complementary to each other since a clinical study without genetic and functional information is only a description of symptoms in which there is a bias given by the physician's specialization. On the other hand, NGS approach allows to identify the mutations potentially involved in the development of the disease, but without any proof of their pathogenicity.

In the past, clinicians considered genetic testing of limited diagnostic value, using such information only if a definitive diagnosis was not given or if it had implications on future family planning. Often the positive results of genetic test did not influence the clinical management of the patient. Thanks to the potentiality of NGS, which allow the parallel sequencing of large multi-genes panels that may describe a broader range of phenotypes, clinicians today are changing their point of view on the role of genetics in patients' care. Nowadays genetic testing may be useful for the evaluation of a clinical case and helps to save time and money in identifying the etiology. An example of this synergy is shown in this work, in which we identified new variants involved in the onset of LDS previously associated with MSSE. Moreover, our study allowed to amplify the phenotypic spectrum associated with mutations in RIPK4 and to broaden the p63 molecular network by adding nectin-4 as a new player.

Lastly, our research led to expand the phenotype resulting from the same mutation in *GJB2*, found in different patients. Our studies suggest that NGS may be incorporated into the medical healthcare system in newborn and prenatal screening, in the presence of familial disorders. We are living in an age of high healthcare costs and early detection of genetic disorders, carrier status, genetic predispositions for cancer and cardiovascular disease could potentially reduce the healthcare costs. On the other hand, the euphoria of the widespread use of the NGS applications to the clinical diagnosis is combined with the awareness of emerging challenges, such as the validation of large number of genetic variations detected. However, beyond this difficulty, NGS is paving the way towards personalized medicine. Indeed, NGS has the potential to generate personalized pharmacogenomics profiles predicting the effects of genes on the individual's response to drugs. The genetic makeup of patients is not completely identical and different genetic mutations can cause the same disease and symptoms. Therefore, the correct diagnosis of a disease and the consideration of the individual's response to a therapeutic agent, which is genetically determined, is crucial. In conclusion, it is paramount in the era of molecular medicine to understand the genetic bases of the diseases and plan a personalized medical approach based on an individual's genetic makeup.

Bibliography

1. McKusick VA. On lumpers and splitters, or the nosology of genetic disease. Perspect Biol Med. 1969 Winter;12(2):298-312.
2. Paaby AB, Rockman MV. The many faces of pleiotropy. Trends Genet. 2013 Feb;29(2):66-73.
3. http://medlineplus.gov/genetics/condition/marfan-syndrome/#causes
4. Van Laer L, Proost D, Loeys BL. Educational paper. Connective tissue disorders with vascular involvement: from gene to therapy. Eur J Pediatr. 2013 Aug;172(8):997-1005.
5. Odofin X, Houbby N, Hagana A, Nasser I, Ahmed A, Harky A. Thoracic aortic aneurysms in patients with heritable connective tissue disease. J Card Surg. 2021 Mar;36(3):1083-1090.
6. García-Martín P, Hernández-Martín A, Torrelo A. Ectodermal dysplasias: a clinical and molecular review. Actas Dermosifiliogr. 2013 Jul-Aug;104(6):451-70. English, Spanish.
7. Verstraeten A, Alaerts M, Van Laer L, Loeys B. Marfan Syndrome and Related Disorders: 25 Years of Gene Discovery. Hum Mutat. 2016 Jun;37(6):524-31.
8. Meester JAN, Verstraeten A, Schepers D, Alaerts M, Van Laer L, Loeys BL. Differences in manifestations of Marfan syndrome, Ehlers-Danlos syndrome, and Loeys-Dietz syndrome. Ann Cardiothorac Surg. 2017 Nov;6(6):582-594.
9. Morton CC, Nance WE. Newborn hearing screening a silent revolution. N Engl J Med. 2006 May 18;354(20):2151-64.
10. Korver AM, Smith RJ, Van Camp G, et al. Congenital hearing loss. Nat Rev Dis Primers. 2017 Jan 12;3:16094.
11. Chari DA, Chan DK. Diagnosis and Treatment of Congenital Sensorineural Hearing Loss. Curr Otorhinolaryngol Rep. 2017 Dec;5(4):251-258.
12. Toriello HV, Reardon W, Gorlin RJ, eds. Hereditary Hearing Loss and Its Syndromes. New York: Oxford University Press; 2004.
13. Chan DK, Chang KW. GJB2-associated hearing loss: systematic review of worldwide prevalence, genotype, and auditory phenotype. Laryngoscope. 2014 Feb;124(2):E34-53.
14. https://medlineplus.gov/genetics/condition/nonsyndromic-hearing-loss/#causes
15. Molster C, Urwin D, Di Pietro L, et al. Survey of healthcare experiences of Australian adults living with rare diseases. Orphanet J Rare Dis. 2016 Mar 24;11:30.
16. Boycott KM, Hartley T, Biesecker LG, at al. A Diagnosis for All Rare Genetic Diseases: The Horizon and the Next Frontiers. Cell. 2019 Mar 21;177(1):32-37.
17. Van Laer L, Dietz H, Loeys B. Loeys-Dietz syndrome. Adv Exp Med Biol. 2014;802:95-105.

18. MacFarlane EG, Parker SJ, Shin JY, et al. Lineage-specific events underlie aortic root aneurysm pathogenesis in Loeys-Dietz syndrome. J Clin Invest. 2019 Feb 1;129(2):659-675.
19. Rojas A, Padidam M, Cress D, Grady WM. TGF-beta receptor levels regulate the specificity of signaling pathway activation and biological effects of TGF-beta. Biochim Biophys Acta. 2009 Jul;1793(7):1165-73.
20. Vander Ark A, Cao J, Li X. TGF-β receptors: In and beyond TGF-β signaling. Cell Signal. 2018 Dec;52:112-120.
21. Loeys BL, Schwarze U, Holm T, et al. Aneurysm syndromes caused by mutations in the TGF-beta receptor. N Engl J Med. 2006 Aug 24;355(8):788-98.
22. MacCarrick G, Black JH 3rd, Bowdin S, et al. Loeys-Dietz syndrome: A primer for diagnosis and management. Genet. Med. 2014;16:576–587
23. Cannaerts E, Kempers M, Maugeri A, et al. Novel pathogenic SMAD2 variants in five families with arterial aneurysm and dissection: further delineation of the phenotype. J Med Genet. 2019 Apr;56(4):220-227.
24. Camerota L, Ritelli M, Wischmeijer A, et al. Genotypic Categorization of Loeys-Dietz Syndrome Based on 24 Novel Families and Literature Data. Genes (Basel). 2019 Sep 28;10(10):764.
25. Cardoso S, Robertson SP, Daniel PB. TGFBR1 mutations associated with Loeys-Dietz syndrome are inactivating. J Recept Signal Transduct Res. 2012 Jun;32(3):150-5.
26. Hara H, Takeda N, Fujiwara T, et al. Activation of TGF-B signaling in an aortic aneurysm in a patient with Loeys-Dietz syndrome caused by a novel loss-of-function variant of TGFBR1. Hum. Genome Var. 2019;6:6. eCollection 2019.
27. Richards S, Aziz N, Bale S, et al. ACMG Laboratory Quality Assurance Committee. Standards and guidelines for the interpretation of sequence variants: a joint consensus recommendation of the American College of Medical Genetics and Genomics and the Association for Molecular Pathology. Genet Med. 2015 May;17(5):405-24.
28. Cannaerts E, Kempers M, Maugeri A, Marcelis C, Gardeitchik T, Richer J, Micha D, Beauchesne L, Timmermans J, Vermeersch P, Meyten N, Chénier S, van de Beek G, Peeters N, Alaerts M, Schepers D, Van Laer L, Verstraeten A, Loeys B. Novel pathogenic *SMAD2* variants in five families with arterial aneurysm and dissection: further delineation of the phenotype. J Med Genet. 2019 Apr;56(4):220-227.
29. Bertoli-Avella AM, Gillis E, Morisaki H, Verhagen JMA, de Graaf BM, van de Beek G, Gallo E, Kruithof BPT, Venselaar H, Myers LA, Laga S, Doyle AJ, Oswald G, van Cappellen GWA, Yamanaka I, van der Helm RM, Beverloo B, de Klein A, Pardo L, Lammens M, Evers C,

Devriendt K, Dumoulein M, Timmermans J, Bruggenwirth HT, Verheijen F, Rodrigus I, Baynam G, Kempers M, Saenen J, Van Craenenbroeck EM, Minatoya K, Matsukawa R, Tsukube T, Kubo N, Hofstra R, Goumans MJ, Bekkers JA, Roos-Hesselink JW, van de Laar IMBH, Dietz HC, Van Laer L, Morisaki T, Wessels MW, Loeys BL. Mutations in a TGF-B ligand, TGFB3, cause syndromic aortic aneurysms and dissections. J Am Coll Cardiol. 2015 Apr 7;65(13):1324-1336.

30. Kornev AP, Taylor SS & Ten Eyck LF. A helix scaffold for the assembly of active protein kinases. Proc. Natl. Acad. Sci. U.S.A. 2008;105:14377–14382.
31. Taylor SS & Kornev AP. Protein kinases: Evolution of dynamic regulatory proteins. Trends Biochem. Sci. 2011;36:65–77.
32. Bowdin SC, Laberge AM, Verstraeten A, Loeys BL. Genetic Testing in Thoracic Aortic Disease--When, Why, and How? Can J Cardiol. 2016 Jan;32(1):131-4.
33. Loeys BL, Dietz HC. Loeys-Dietz Syndrome. 2008 Feb 28 [updated 2018 Mar 1]. In: Adam MP, Ardinger HH, Pagon RA, Wallace SE, Bean LJH, Gripp KW, Mirzaa GM, Amemiya A, editors. GeneReviews® [Internet]. Seattle (WA): University of Washington, Seattle; 1993–2022. PMID: 20301312.
34. Busa T, Jeraiby M, Clémenson A, at al. Confirmation that RIPK4 mutations cause not only Bartsocas-Papas syndrome but also CHAND syndrome. Am J Med Genet A. 2017 Nov;173(11):3114-3117.
35. Brancati F, Fortugno P, Bottillo I, et al. Mutations in PVRL4, encoding cell adhesion molecule nectin-4, cause ectodermal dysplasia-syndactyly syndrome. Am J Hum Genet. 2010 Aug 13;87(2):265-73.
36. Leslie EJ, O'Sullivan J, Cunningham ML, et al. Expanding the genetic and phenotypic spectrum of popliteal pterygium disorders. Am J Med Genet A. 2015 Mar;167A(3):545-52.
37. Kalay E, Sezgin O, Chellappa V, at al. Mutations in RIPK4 cause the autosomal-recessive form of popliteal pterygium syndrome. Am J Hum Genet. 2012 Jan 13;90(1):76-85.
38. Mitchell K, O'Sullivan J, Missero C, at al. Exome sequence identifies RIPK4 as the Bartsocas-Papas syndrome locus. Am J Hum Genet. 2012 Jan 13;90(1):69-75.
39. Gollasch B, Basmanav FB, Nanda A, et al. Identification of a novel mutation in RIPK4 in a kindred with phenotypic features of Bartsocas-Papas and CHAND syndromes. Am J Med Genet A. 2015 Nov;167A(11):2555-62.
40. Busa T, Jeraiby M, Clémenson A, at al. Confirmation that RIPK4 mutations cause not only Bartsocas-Papas syndrome but also CHAND syndrome. Am J Med Genet A. 2017 Nov;173(11):3114-3117.

41. Meylan E, Tschopp J. The RIP kinases: crucial integrators of cellular stress. Trends Biochem Sci. 2005 Mar;30(3):151-9.
42. Chen L, Haider K, Ponda M, at al. Protein kinase C-associated kinase (PKK), a novel membrane-associated, ankyrin repeat-containing protein kinase. J Biol Chem. 2001 Jun 15;276(24):21737-44.
43. Kwa MQ, Huynh J, Aw J, Zhang L, Nguyen T, Reynolds EC, Sweet MJ, Hamilton JA, Scholz GM. Receptor-interacting protein kinase 4 and interferon regulatory factor 6 function as a signaling axis to regulate keratinocyte differentiation. J Biol Chem. 2014 Nov 7;289(45):31077-87.
44. Moretti F, Marinari B, Lo Iacono N, Botti E, Giunta A, Spallone G, Garaffo G, Vernersson-Lindahl E, Merlo G, Mills AA, Ballarò C, Alemà S, Chimenti S, Guerrini L, Costanzo A. A regulatory feedback loop involving p63 and IRF6 links the pathogenesis of 2 genetically different human ectodermal dysplasias. J Clin Invest. 2010 May;120(5):1570-7.
45. Richardson R, Mitchell K, Hammond NL, Mollo MR, Kouwenhoven EN, Wyatt ND, Donaldson IJ, Zeef L, Burgis T, Blance R, van Heeringen SJ, Stunnenberg HG, Zhou H, Missero C, Romano RA, Sinha S, Dixon MJ, Dixon J. p63 exerts spatio-temporal control of palatal epithelial cell fate to prevent cleft palate. PLoS Genet. 2017 Jun 12;13(6):e1006828.
46. Parsa R, Yang A, McKeon F, Green H. Association of p63 with proliferative potential in normal and neoplastic human keratinocytes. J Invest Dermatol. 1999 Dec;113(6):1099-105.
47. Brancati F, Agolini E, Fortugno P. Nectinopathies: an emerging group of ectodermal dysplasia syndromes. G Ital Dermatol Venereol. 2013 Feb;148(1):59-64. PMID: 23407077.
48. Gripp KW, Ennis S, Napoli J. Exome analysis in clinical practice: expanding the phenotype of Bartsocas-Papas syndrome. Am J Med Genet A. 2013 May;161A(5):1058-63.
49. Mollo MR, Antonini D, Mitchell K, et al. p63-dependent and independent mechanisms of nectin-1 and nectin-4 regulation in the epidermis. Exp Dermatol. 2015 Feb;24(2):114-9.
50. Aasen T. Connexins, Innexins, and Pannexins: From Biology to Clinical Targets. Biomolecules. 2021 Jan 25;11(2):155.
51. Lawrence TS, Beers WH, Gilula NB. Transmission of hormonal stimulation by cell-to-cell communication. Nature. 1978 Apr 6;272(5653):501-6.
52. Goodenough DA, Paul DL. Beyond the gap: functions of unpaired connexon channels. Nat Rev Mol Cell Biol. 2003 Apr;4(4):285-94.
53. Harris AL. Emerging issues of connexin channels: biophysics fills the gap. Q Rev Biophys. 2001 Aug;34(3):325-472. Erratum in: Q Rev Biophys 2002 Feb;35(1):109.

54. Jiang JX, Gu S. Gap junction- and hemichannel-independent actions of connexins. Biochim Biophys Acta. 2005 Jun 10;1711(2):208-14.
55. Sáez JC, Retamal MA, Basilio D, Bukauskas FF, Bennett MV. Connexin-based gap junction hemichannels: gating mechanisms. Biochim Biophys Acta. 2005 Jun 10;1711(2):215-24.
56. Wiszniewski L, Limat A, Saurat JH, Meda P, Salomon D. Differential expression of connexins during stratification of human keratinocytes. J Invest Dermatol. 2000 Aug;115(2):278-85.
57. Meşe G, Richard G, White TW. Gap junctions: basic structure and function. J Invest Dermatol. 2007 Nov;127(11):2516-24.
58. Lee JR, White TW. Connexin-26 mutations in deafness and skin disease. Expert Rev Mol Med. 2009 Nov 19;11:e35.
59. Shearer AE, Hildebrand MS, Smith RJH. Hereditary Hearing Loss and Deafness Overview. 1999 Feb 14 [updated 2017 Jul 27]. In: Adam MP, Ardinger HH, Pagon RA, Wallace SE, Bean LJH, Gripp KW, Mirzaa GM, Amemiya A, editors. GeneReviews® [Internet]. Seattle (WA): University of Washington, Seattle; 1993–2022. PMID: 20301607.
60. Brown CW, Levy ML, Flaitz CM, Reid BS, Manolidis S, Hebert AA, Bender MM, Heilstedt HA, Plunkett KS, Fang P, Roa BB, Chung P, Tang HY, Richard G, Alford RL. A novel GJB2 (connexin 26) mutation, F142L, in a patient with unusual mucocutaneous findings and deafness. J Invest Dermatol. 2003 Nov;121(5):1221-3.
61. Ibáñez MM, Alcalde MM, Jiménez MR, Muñoz MD, Díez-Delgado FJ. An unusual mucocutaneous syndrome with sensorineural deafness due to connexin 26 mutations. Pediatr Dermatol. 2013 Nov-Dec;30(6):e138-42.
62. Lazic T, Li Q, Frank M, Uitto J, Zhou LH. Extending the phenotypic spectrum of keratitis-ichthyosis-deafness syndrome: report of a patient with GJB2 (G12R) Connexin 26 mutation and unusual clinical findings. Pediatr Dermatol. 2012 May-Jun;29(3):349-57.
63. White TW. Functional analysis of human Cx26 mutations associated with deafness. Brain Res Brain Res Rev. 2000 Apr;32(1):181-3.
64. Bruzzone R, Veronesi V, Gomès D, Bicego M, Duval N, Marlin S, Petit C, D'Andrea P, White TW. Loss-of-function and residual channel activity of connexin26 mutations associated with non-syndromic deafness. FEBS Lett. 2003 Jan 2;533(1-3):79-88.
65. Gerido DA, White TW. Connexin disorders of the ear, skin, and lens. Biochim Biophys Acta. 2004 Mar 23;1662(1-2):159-70.

66. van Steensel MA. Gap junction diseases of the skin. Am J Med Genet C Semin Med Genet. 2004 Nov 15;131C(1):12-9. Erratum in: Am J Med Genet C Semin Med Genet. 2006 Feb 15;142(1):58.
67. Richard G. Connexin disorders of the skin. Clin Dermatol. 2005 Jan-Feb;23(1):23-32.
68. Lai-Cheong JE, Arita K, McGrath JA. Genetic diseases of junctions. J Invest Dermatol. 2007 Dec;127(12):2713-25.
69. García IE, Prado P, Pupo A, Jara O, Rojas-Gómez D, Mujica P, Flores-Muñoz C, González-Casanova J, Soto-Riveros C, Pinto BI, Retamal MA, González C, Martínez AD. Connexinopathies: a structural and functional glimpse. BMC Cell Biol. 2016 May 24;17 Suppl 1(Suppl 1):17.
70. Iossa S, Marciano E, Franzé A. GJB2 Gene Mutations in Syndromic Skin Diseases with Sensorineural Hearing Loss. Curr Genomics. 2011 Nov;12(7):475-785.
71. Hervé JC, Bourmeyster N, Sarrouilhe D. Diversity in protein-protein interactions of connexins: emerging roles. Biochim Biophys Acta. 2004 Mar 23;1662(1-2):22-41.

Publications co-authored by Rosanna Monetta

Camerota L, Ritelli M, Wischmeijer A, Majore S, Cinquina V, Fortugno P, **Monetta R**, Gigante L, Marfan Syndrome Study Group Tor Vergata University Hospital, Sangiuolo FC, Novelli G, Colombi M, Brancati F. Genotypic Categorization of Loeys-Dietz Syndrome Based on 24 Novel Families and Literature Data. Genes (Basel). 2019 Sep 28;10(10):764. doi: 10.3390/genes10100764. PMID: 31569402; PMCID: PMC6826414.

Guerra L, Bergamo F, D'Apice MR, Angelucci F, di Girolamo S, Camerota L, **Monetta R**, Annessi G, Castiglia D, Novelli G, Paradisi M, Brancati F. Keratoderma-Deafness-Mucocutaneous Syndrome Associated with Phe142Leu in the GJB2 Gene. Acta Derm Venereol. 2019 Nov 1;99(12):1192-1194. doi: 10.2340/00015555-3291. PMID: 31408183.

Li D, March ME, Fortugno P, Cox LL, Matsuoka LS, **Monetta R**, Seiler C, Pyle LC, Bedoukian EC, Sánchez-Soler MJ, Caluseriu O, Grand K, Tam A, Aycinena ARP, Camerota L, Guo Y, Sleiman P, Callewaert B, Kumps C, Dheedene A, Buckley M, Kirk EP, Turner A, Kamien B, Patel C, Wilson M, Roscioli T, Christodoulou J, Cox TC, Zackai EH, Brancati F, Hakonarson H, Bhoj EJ. Pathogenic variants in CDH11 impair cell adhesion and cause Teebi hypertelorism syndrome. Hum Genet. 2021 Jul;140(7):1061-1076. doi: 10.1007/s00439-021-02274-3. Epub 2021 Apr 3. PMID: 33811546.

Fortugno P, **Monetta R**, Belli M, Botti E, Angelucci F, Palmerini MG, Annarita NS, De Luca C, Ceccarini M, Salvatore M, Bianchi L, Macioce P, Teson M, Ricci F, Network IUD, Macchiarelli G, Didona B, Costanzo A, Castiglia D, Brancati F. RIPK4 regulates cell-cell adhesion in epidermal development and homeostasis. Hum Mol Genet. 2022 Feb 26:ddac046. doi: 10.1093/hmg/ddac046. Epub ahead of print. PMID: 35220430.

List of abbreviations

FBN-1	Fibrillarin-1
TGFβ	Transforming grow factor beta
TGFBR1/2	Transforming grow factor receptor beta 1/2
SMAD2/3	SMAD family members 2/3
EDs	Ectodermal dysplasias
EDAR	Ectodysplasin A receptor
HCTD	Hereditable Connective Tissue Disorders
COL1A1	Collagen type I alpha 1 chain
COL3A1	Collagen type III alpha 1 chain
COL5A1	Collagen type V alpha 1 chain
BGN	Biglycan
ADAMTS2	ADAM metallopeptidase with thrombospondin type 1 motif 2
PLOD1	Procollagen-lysine, 2-oxoglutarate 5-dioxygenase 1
ECM	Extracellular matrix
MFS	Marfan syndrome
EDS	Ehlers-Danlos syndrome
LDS	Loeys-Dietz syndrome
CMV	Cytomegalovirus
SNHL	Congenital sensorineural hearing loss
GJB2	Gap Junction protein beta 2
CX26	Gap Junction protein beta 2
NGS	Next Generation Sequencing
TAAD	Thoracic aortic aneurysms dissections
SMAD4	SMAD family member 4
PI3K	Phosphatidylinositol-4,5-bisphosphate 3-kinase catalytic subunit beta
AKT	AKT serine/threonine kinase 1
p38 MAPK	Mitogen-activated protein kinase 14
MAPK-ERK	Mitogen-activated protein kinase 1
JNK	Mitogen-activated protein kinase 8
MSSE	Multiple self-healing squamous epithelioma
NMD	Nonsense-mediated mRNA decay
ACMG	American College of Medical Genetics

DXA	Dual X-ray absorptiometry
CT	Computed tomography
dbSNP	Single nucleotide polymorphism database
gnomAD	Genome aggregation database
LOVD	Leiden Open Variation Database
HGMD	Human Gene Mutation Database
ATP	Adenosine triphosphate
EPK	Eukaryote protein kinase
SP	Signal peptide
TM	Transmembrane domain
GS	Glycine- and serine-rich sequence domain
WB	Western blot
IF	Immunofluorescence
α-SMA	Actin alpha 2, smooth muscle
VINC	Vinculin
GAPDH	Glyceraldehyde-3-phosphate dehydrogenase
TP63	Tumor proteion 63
IRF6	Interferon regulatory factor 6
PVRL4	Poliovirus receptor-related protein 4
RIPK4	Receptor interacting serine/threonine kinase 4
BPS	Bartsocas-Papas syndrome
PPS	Popliteal pterygium syndrome
CHAND	Curly hair-ankyloblepharon-nail dysplasia syndrome
EDSS1	Ectodermal dysplasia syndactyly syndrome
HEK293	Human embryonic kidney 293
WT	Wild type
CIP	Calf Intestinal phosphatase
PMA	Phorbol 12-myristate 13-acetate
PKC	Proline rich transmembrane protein 2
PKP1	Plakophilin-1
DSG1	Desmoglein
NCBI	National Center for Biotechnology Information
cAMP	Cyclic adenosine monophosphate
cGMP	Cyclic guanosine monophosphate

IP3	Inositol 1,4,5-trisphosphate
Cx46	Gap Junction protein alpha 3
Cx50	Gap Junction protein alpha 8
Cx30	Gap Junction protein beta 6
Cx30.3	Gap Junction protein beta 4
Cx31	Gap Junction protein beta 3
Cx43	Gap Junction protein alpha1
TM	Transmembrane domain
EC	Extracellular loop
CL	Cytoplasmic loop
BPS	Bart-Pumphrey syndrome
HID	Hystrix-like ichthyosis with deafness
KID	Keratitis-ichthyosis-deafness syndrome
PPK	Keratoderma palmoplantar with deafness
VS	Vohwinkel syndrome

Acknowledgment

Se non l’avessi incontrata, avrei perso tanto. Durante il mio percorso di dottorato non ho capito il perché di molte cose, poi mi si sono svelate. Mi ha insegnato quello in cui io non ero avvezza. Grazie a lei non ho paura di un foglio bianco. Lei mi ha dato la forza di seguire i miei sogni e di affrontare le difficoltà anche se fa paura. Grazie a lei ho avuto la possibilità di conoscere Paola.

Paola tu mi hai insegnato tutto quello che so. Con pazienza materna mi hai dato i mezzi per sviluppare una mente critica (almeno spero). Mi hai sempre dato la possibilità di mettermi alla prova, mi hai spronato in tutte le situazioni, hai fatto si che diventassi indipendente e che riuscissi a gestire il mio lavoro non facendomi sentire mai sola. Per me è stato un onore poter imparare da te.

In questi anni, nonostante tanti errori, ho cercato di imparare il più possibile.

Ringrazio il Professore Silvio Romano per avermi seguito in questi anni.

Ringrazio gli amici e i colleghi che sono sempre stati pronti a sopportarmi e supportarmi.

Un ringraziamento speciale va ad A. per avermi capito, aiutato, sopportato e per esserci sempre stato.